Aus der Neurochirurgischen Klinik und Poliklinik

Klinikum der Ludwig-Maximilians-Universität München

Vorstand: Prof. Dr. Jörg-Christian Tonn

The diversity of tumor-associated cells in primary and recurrent glioblastoma

Dissertation

zum Erwerb des Doktorgrades der Medizin

an der Medizinischen Fakultät der

Ludwig-Maximilians-Universität zu München

Vorgelegt von

Dongxu Zhao

Aus

Henan, P.R. China

2021

Mit Genehmigung der Medizinischen Fakultät

der Universität München

Berichterstatter: Prof. Dr. Rainer Glaß

Mitberichterstatter: Prof. Dr. Dr. Michael von Bergwelt

Dr. Dr. Sabine Liebscher

Prof. Dr. Nathalie Albert

Mitbetreuung durch den

promovierten Mitarbeiter: Dr. Roland Kälin

Dekan: Prof. Dr. med. Thomas Gudermann

Tag der mündlichen Prüfung: 02.12.2021

Eidesstattliche Versicherung

Zhao, Dongxu

Name, Vorname

Ich erkläre hiermit an Eides statt,

dass ich die vorliegende Dissertation mit dem Thema

The diversity of tumor-associated cells in primary and recurrent glioblastoma

selbständig verfasst, mich außer der angegebenen keiner weiteren Hilfsmittel bedient und alle Erkenntnisse, die aus dem Schrifttum ganz oder annähernd übernommen sind, als solche kenntlich gemacht und nach ihrer Herkunft unter Bezeichnung der Fundstelle einzeln nachgewiesen habe.

Ich erkläre des Weiteren, dass die hier vorgelegte Dissertation nicht in gleicher oder in ähnlicher Form bei einer anderen Stelle zur Erlangung eines akademischen Grades eingereicht wurde.

Munich, 25.03.2021 — Zhao Dongxu

Ort, Datum — Unterschrift Doktorandin/Doktorand

I. Contents

II. List of figures

III. List of tables

IV. Abbreviations

BBB	Blood brain barrier
BDNF	Brain-derived neurotrophic factor
CDKN2A	Cyclin-dependent kinase Inhibitor 2A
CNS	Central nervous system
CSF 1	Colony stimulating factor 1
DPO	Day post-operatively
EGFR	Epidermal growth factor receptor
GBM	Glioblastoma multiforme
GCV	Ganciclovir
GSCs	Glioma stem cells
HSVTK	Herpes simplex virus thymidine kinase
IDH 1	Isocitrate dehydrogenase 1
MMP	Metalloprotease
NF1	Neurofibromatosis type 1
NLGN3	Soluble neuroligin-3
NPC	Neural precursor cells
OPC	Oligodendrocyte precursor cells
PDGF	Platelet-derived growth factor
PDGFRA	Platelet-derived growth factor receptor-α
PDGFRβ	Platelet derived growth factor receptor B

PFA	Paraformaldehyde
PTEN	Phosphatase and tensin homolog
scRNA-seq	Single cell RNA sequencing
SVZ	Subventricular zone
TAMEP	Tumor associated cells with a myeloid-like expression profile
TAMs	Tumor associated myeloid cells
TCGA	The Cancer Genome Atlas
TGF-β	Transforming growth factor β
TIMP	Tissue inhibitor of metalloproteinase
t-SNE	t-distributed stochastic neighbor embedding
VEGF	Vascular endothelial growth factor
WHO	World Health Organization

1. Introduction

1.1 Glioblastoma

Glioblastoma multiforme (GBM) is the most common and malignant tumor presenting in the central nervous system (CNS), and prognosis for GBM patients remains very poor[1-3]. Despite the development of innovative diagnostics and new therapies, patients diagnosed with GBM have a median survival of only 15 months [4]. Standard GBM treatment includes maximal surgical dissection, followed by radiotherapy and chemotherapy. However, GBM often develops treatment resistance due to tumor heterogeneity[5-7]. Moreover, complete surgical resection is often difficult to achieve depending on tumor location and due to its highly invasive nature[8]. Residual tumor cells can lead to malignant progression and recurrence[9].

1.2 Classification of glioblastoma

According to the World Health Organization (WHO) classification in 2016 [10], glioblastomas are divided into two subgroups: primary and secondary GBM. Primary GBM account for nearly 90% of total GBM cases and develop rapidly, and are not associated with mutation of in the isocitrate dehydrogenase 1 (*IDH 1*) gene [11]. The remaining 10% of cases comprise secondary GBM, which progress from a low-grade diffuse astrocytoma or anaplastic astrocytoma and carry the *IDH 1* mutation[12]. Patients afflicted with secondary GBM are usually younger and have a better

prognosis[13, 14].

Analysis of GBM expression profiles has been achieved using high-throughput sequencing technologies that have been developed in the last decades [15-17]. Based on genetic differences identified in the Cancer Genome Atlas (TCGA), GBM can be classified into four subgroups: classical, mesenchymal, proneural and neural [18, 19]. Classical glioblastoma is characterized by increased expression of the epidermal growth factor receptor (*EGFR*) and loss of phosphatase and tensin homolog (*PTEN*) and cyclin-dependent kinase Inhibitor 2A (*CDKN2A*)[20], and it is highly responsive to radiotherapy and chemotherapy[21]. The mesenchymal subtype is characterized by mutations in Neurofibromatosis type 1 (*NF1*), tumor protein 53 (TP53), and *PTEN*, and is associated with worse outcome[22, 23]. Signature genetic alterations in proneural glioblastoma tumors include overexpression of controlling CNS development genes such as platelet-derived growth factor receptor-α (*PDGFRA*) [24]. The neural subtype likely is an artifact due to contamination with parenchymal cells and no longer considered as an independent GBM subtype[25].

1.3 Glioblastoma treatment

Surgical resection is the first therapeutic choice in glioblastoma. The preferred strategy is maximal surgical removal consistent with preserving the neurologic function[26, 27]. In some situations, where the patient's clinical condition does not permit operation or the tumor location is not amenable to resection, subtotal resection or biopsy is also

required[28, 29]. Molecular characterizations of glioblastoma, such as *IDH1* mutation, O^6-methylguanine-DNA methyltransferase（*MGMT*）promoter methylation as well as telomerase reverse transcriptase（*TRET*）promoter mutation are increasingly used to guide the post-operative treatment[19]. MGMT promoter methylation is predictive of GBM benefiting from alkylating agent chemotherapy. For patients with *MGMT*-methylated glioblastoma, who are younger than 70 years of age, the use of temozolomide, combined with radiation therapy is recommended[30]. An open-label trial conducted by the European Organization for Research and Treatment of Cancer/National Cancer Institute of Canada （EORTC/NCIC）showed combined therapy could largely improve the median survival as compared to radiotherapy alone[31]. Adjuvant temozolomide treatment benefited all patient subsets, including those older patients and those with other poor prognostic factors[32-34]. For patients who have *MGMT*-unmethylated glioblastoma and are younger than 70 years of age, they had a poor response to standard therapies, thus leading to a poor prognosis[30]. These patients were encouraged to participate in clinical trials. For those patients who are older than 70 years, temozolomide, combined with shorter course radiation can be given after evaluation of postoperative functional status and *MGMT* status [35].

Now various therapies such as immunotherapy and vaccine-based therapies are being explored in clinical trials for patients with glioblastoma. But only two therapies, bevacizumab and tumor-treating fields (TT fields) were approved by the Food and Drug Administration（FDA）until now[36, 37]. Bevacizumab is a monoclonal antibody, which targets VEGFA and thereby inhibits angiogenesis. Although bevacizumab only

extended progression-free survival（PFS） and not overall survival（OS）, it had an anti-edema effect and improved clinical parameters[38]. Furthermore, bevacizumab had been used in the treatment of recurrent glioblastoma, in combination with radiation and chemotherapy, which largely increased PFS in patients[36]. TT field treatment is a non-invasive anti-cancer therapy, which may inhibit tumor growth and proliferation through interfering with biological mechanisms, including mitosis, DNA repair, and autophagy[39]. Several clinical trials showed that this new therapy may extend PFS and OS in primary and recurrent glioblastoma[40, 41].

1.4 Glioblastoma recurrence

Glioblastoma relapse even after aggressive treatment [42]. Roughly two-thirds of recurrent glioblastoma relapse within 2 cm of the primary tumor margin[43, 44]. One-third of glioblastoma recur at distant sites, including different brain lobes or even infratentorial locations[45]. Several major reasons account for tumor recurrence[46, 47]: 1) GBM are infiltrative and invasive, making complete surgical resection difficult; 2) the intratumoral heterogeneity in glioblastoma supports chemo- and irradiation- therapy resistance; 3) glioblastoma stem cells (GSCs), characterized by their self-renewal, persistent proliferation, and high capacity for tumor initiation, represent a major source for relapsing GBM.

There is no unified and well-defined treatment in recurrent glioblastoma. Re-excision still remains a vital therapeutic approach, but the tumor size and location, patients'

clinical condition, and other factors permit only a small proportion of patients for a substantial surgical resection[48]. If re-excision is not possible, re-irradiation, chemotherapy, immunotherapy, TT fields treatment, and other novel treatment methods are also recommended[49].

When comparing the differences between primary and corresponding recurrent glioblastoma, researchers found the majority of mutations were retained[50, 51]. However, in distant recurrence, mutation-retention was much lower[52]. Despite many significant developments in the research and treatment of primary glioblastomas, much less is known about the unique molecular characterization of recurrent glioblastoma. The fact that re-excision is not often performed largely hinders the comparison between primary and matched recurrence, which is one caveat for our understanding of tumor recurrence[53]. A wide variety of GBM models are developed to explore primary tumorigenesis, underlying mechanisms of treatment resistance in primary GBM. Lack of mouse models generating recurrent tumors of relevant anatomical location made it difficult to identify how clonal subpopulations within primary GBM escape therapy and develop tumor recurrence[7].

1.5 The diverse tumor-parenchymal cells in the glioblastoma environment

Now a lot of studies focus on the interactions between GBM tumor cells and their surrounding cells, including normal brain cells and immune cells immigrating from the blood stream[54, 55]. GBM recruits several parenchymal cell types into its tumor

environment, thereby promoting tumor progression and growth and potentially modifying tumor responses to treatment [56-58].

Tumor-associated myeloid cells (TAMs), including microglia and peripheral blood-derived macrophages, accumulate in GBM during tumor progression [59, 60]. In the healthy brain, microglia are the primary innate immune cells and regulate brain development and behavioral functions[61]. Microglia derive from yolk sac progenitors and constitute a self-maintained life-long cell population without contribution from peripheral macrophages under physiological conditions[62]. However, bone-marrow-derived macrophages can infiltrate the brain tumor area due to disruption of the blood-brain-barrier (BBB). Bone-marrow derived macrophages originate from hematopoietic stem cells and have a much shorter half-life than microglia[63]. Microglia and bone-marrow derived macrophages have large overlapping marker profile[64, 65]. In disease-free conditions, microglia and peripheral macrophages could be distinguished by CD11b and CD45 expression level[66, 67]. But in glioblastoma, the CD molecule expression in TAMs is altered[65, 68]. Now several specific markers of microglia are applied to distinguish microglia from peripheral macrophages[69-71]. Furthermore, genetic mouse models that indicate developmental markers specifically for microglia or peripheral macrophages are generated and distinct myeloid-cell populations could be observed[72, 73]. The number of TAMs in glioblastoma is high and can constitute up to 30% of the tumor mass[64] and they play major roles in tumor progression through enhancement of glioblastoma invasion and angiogenesis[57, 64]. Several factors released by tumor cells, such as colony-stimulating factor 1 (CSF 1) and

monocyte chemoattractant protein-1 (MCP-1), attract TAMs, leading to their intratumoral accumulation, and can convert them into a tumor-supporting phenotype [65, 74, 75]. Activated TAMs promote metalloprotease (MMP) activity and suppress tissue inhibition of metalloproteinase (TIMP)-2 expression, leading to extracellular matrix degradation and facilitating tumor invasion[76]. TAMs can also affect glioma stem cells (GSCs), which are a small cell population with self-renewal and multi-lineage differentiation properties[77, 78]. Tumor growth factor β (TGF-β), released from TAMs, increases GSCs invasiveness[76]. Enhanced activity of MMPs expressed by TAMs can promote glioblastoma angiogenesis by modifying the extracellular matrix on blood vessels[79]. Additionally, TAMs promote the release of stem cell factor, which attracts bone-marrow derived endothelial progenitors to support vasculogenesis[80]. TAMs also overexpress molecules such as VEGF and CXCL2 that have direct pro-angiogenic effects[60, 81].

Glioblastoma is additionally characterized by extensive angiogenesis[82]. A dense network of tortuous and leaky vessels with dilated lumen and abnormally thickened basement membranes represents a hallmark of GBM[83]. Glioma and immune cells release various factors that promote angiogenesis, including vascular endothelial growth factor (VEGF), platelet-derived growth factor (PDGF), integrins, and angiopoietins[76, 84-87]. Recent studies show that GSCs present another source of vascular constituents and can differentiate into endothelial cells and pericytes, thus contributing to vessel formation[88-90]. VEGF is highly expressed in gliomas and correlates with tumor malignancy[91, 92]. Endothelial cells express the vascular

endothelial growth factor receptor 2 (VEGFR2), which, together with VEGF expression, establishes a paracrine signaling loop resulting in endothelial cell proliferation and migration [93]. Ultimately, the increased glioma VEGF signaling pathway results in decreased vessel and vascular integrity due to disruption of the BBB[94]. The BBB is composed of endothelial cells, pericytes, and astrocytes, together forming the so-called neurovascular unit that maintains brain homeostasis by regulating ion and molecular transfer between the brain and blood[94]. The abnormal or disrupted BBB in glioma causes non-uniform permeability and active efflux of various molecules into the tumor tissue, leading to cerebral edema[94]. These pathological changes also attract immune cells, such as macrophages, which further promote angiogenesis and brain infiltration of peripheral leukocytes into poorly perfused areas. Multiple strategies are currently developed to normalize the GBM vasculature, to reduce myeloid-cell accumulation and to improve the delivery of therapeutics into the tumor [95-97].

Furthermore, many other examples of interactions between glioblastoma cells and their surrounding cells, such as T cells and astrocytes, within the tumor microenvironment have been reported [98, 99]. These new insights provide the basis for potential novel therapies for gliomas[100].

1.6 The heterogeneity of glioblastoma

GBM heterogeneity, which supports tumor progression, treatment resistance, metastasis, and recurrence, is one of the fundamental characteristics in glioblastoma[6, 7]. There are two types of heterogeneity: inter-individual and intra-tumoral

heterogeneity. Although glioblastomas are classified into several subtypes according to their genetic alterations, recent studies show different regions in the same tumor display distinct transcriptional profiles [101, 102]. This intra-tumoral heterogeneity is likely caused by spatial differences in growth factors, oxygen pressure, blood vessel density, and extracellular matrix composition within the tumor microenvironment[103, 104]. TAMs also contribute to the heterogeneity of glioma[105]. The degree of macrophage infiltration varies in glioblastoma subtypes and the gene signature of bone-marrow derived macrophages is correlated with poor survival in low grade gliomas[106]. The analysis of microglia- and macrophage- specific marker genes showed a microglia signature enriched in the leading edge of gliomas, while phagocytes from tumor core have an expression-profile of monocyte derived macrophages[107]. Since only a single piece of the tumor is usually used for clinical diagnosis and the following treatment, neuro-oncologists may receive an incomplete and possibly misleading diagnosis because of the regional heterogeneity[108, 109]. Therefore, understanding mechanism of GBM heterogeneity and how GBM environment causes GBM heterogeneity are essential for developing personalized glioblastoma treatments[110-112].

1.7 Objectives of the study

a) Investigate the role of NPC progeny in GBM progression;

b) Assess TAMEP presence and its heterogeneity in human brain tumor tissue;

c) Establish a feasible recurrent GBM mouse model;

d) Compare the heterogeneous features between primary and recurrent glioblastoma.

2. Materials

2.1 Equipment and Devices

Table 2.1 Equipment and Devices

Equipment/Device	**Company**
Incubator	Thermo Fisher Scientific
Fridge (4°C, -20°C, -80°C)	LIEBHERR
Water bath	Memmert
Hera safe hood	Thermo Fisher Scientific
Centrifuge	Thermo Fisher Scientific
Stereotactic frame	Stereotactic Frame
Countess II FL automated cell counter	Thermo Fisher Scientific
Microliter syringe	Hamilton
Surgical instruments	Aesculap
Perfusion system dose IT P910	Integra Biosciences AG
Micropipette (10µl, 20µl, 100µl, 200µl, 1000µl)	Eppendorf
Digital vortex mixer	VWR
Microtome slide 2003	PFM medical AG
Pipette boy	Eppendorf
Magnetic hotplate stirrer	VWR
Microscope Axioskop 2	Carl Zeiss
Microscope Axiovert 25	Carl Zeiss
Microscope camera Axiocam MRm	Carl Zeiss
Leica SP8X WLL upright confocal	Leica Microsystems

microscope	
Leica DMI8 inverted fluorescent microscope	Leica Microsystems
Leica M205 FA stereo microscope	Leica Microsystems
Axiovision Rel. 4.8 / 4.9 software	Carl Zeiss

2.2 Reagents and chemicals

Table 2.2 Reagents and chemicals

Product	**Supplier**	**Catalog number**
Paraformaldehyde (PFA)	Sigma Aldrich	158127
Sucrose	Sigma Aldrich	S0389
Roti® Histol	Carl Roth	6640.2
Ethanol 100%	CLN GmbH	20705911
Ethanol 70%	CLN GmbH	28012019
Ethanol 96%	CLN GmbH	25062018
Entellan® mounting medium	Merck	107960
Acetone 100%	Sigma Aldrich	179124
DAPI	Sigma Aldrich	D9542
Donkey serum	Jackson ImmunoResearch	017-000-121
2,2,4-Trimethylpentane	Thermo Fisher Scientific	10254210
Fluorescence Mounting Medium	Dako	S3023
Ethylene glycol	Sigma Aldrich	324558
HCl	Sigma Aldrich	320331
Isopropanol	Sigma Aldrich	34863
Ketamin 10%	Zoetis Deutschland GmbH	402527
Mayer's Hematoxylin Solution	Carl Roth	T865.2

NaCl 0.9%	B. Braun Melsungen AG	3570350
PBS	Apotheke Klinikum der Universität München	ST016
Rompun 2%	Bayer	770-081
Triton X-100	Roche Diagnostics	T8787
Tween-20	Sigma Aldrich	P9416
Tamoxifen	Sigma Aldrich	T5648
Corn Oil	Sigma Aldrich	C8267
Ganciclovir	Sigma Aldrich	G2536
Bepanthen® Eye- and Nose-cream	Bayer Vital GmbH	1578681

2.3 Cell culture materials

Table 2.3 Cell culture materials

Material	**Catalog Number**	**Supplier**
DMEM	FG0415	Biochrom
Fetal Bovine Serum	10270-106	Life Technologies
MEM non-essential amino acids	11140-035	Life Technologies
Penicillin-streptomycin	15140-122	Life Technologies
Trypan Blue Solution 0.4%	T8154	Sigma Aldrich
Trypsin/EDTA	L2153	Merck Millipore

2.4 Consumables

Table 2.4 Consumables

Product	**Supplier**	**Catalog Number**
Cell Culture Flask (T25)	TPP	90026

Cell Culture Flask (T75)	TPP	90076
Cell Culture Flask (T150)	TPP	90151
Centrifuge tubes (0.5ml)	Eppendorf	0030123301
Centrifuge tubes (1.5ml)	Eppendorf	0030123611
Centrifuge tubes (2ml)	Eppendorf	0030123344
Centrifuge tubes (15ml)	TPP / Falcon	91015
Centrifuge tubes (50ml)	TPP / Falcon	91050
Cover slips	Gerhard Menzel	BB022050A1
Ethibond excel (5-0) sutures	Ethicon	D8867
Microtome Blade A35	Feather	207500011
Dako-pen	Dako	S2002
Pipette tips (10µl)	Eppendorf	0030000811
Pipette tips (200µl)	Eppendorf	0030000889
Pipette tips (1000µl)	Eppendorf	0030000927
Plate (12 wells)	TPP	92012
Plate (24 wells)	TPP	92024
Scalpel (#15)	Feather	200130015
Scalpel (#23)	Feather	200130023
Slide for immunolabeling	Gerhard Menzel	J1800AMNZ
Stripette™ serological pipets (5ml)	Corning	4051
Stripette™ serological pipets (10ml)	Corning	4488
Stripette™ serological pipets (25ml)	Corning	4251
Syringe (1ml)	B. Braun Melsungen AG	9166017V
Syringe needle (27G)	B. Braun Melsungen AG	9186174
Syringe needle (30G)	B. Braun Melsungen AG	4656300

Tissue-Tek Cryomold (15mm×15mm×5mm)	Sakura Finetek	10690461

2.5 Primary Antibodies

Table 2.5 Primary antibodies

Immunogen	**Host Species**	**Dilution**	**Catalog number**	**Provider**
PDGFRβ	Goat	1:200	AF1042	R&D Systems
CD31	Rat	1:50	550274	Becton Dickinson
Iba 1	Goat	1:400	ab5076	Abcam
Iba 1	Rabbit	1:400	019-19741	Wako Pure
Sox2	Rabbit	1:200	ab97959	Abcam
Sox2	Goat	1:200	AF2018	Novos
PU.1	Rabbit	1:100	2258s	Cell Signaling
CD11b	Rabbit	1:400	ab52478	Abcam

2.6 Secondary Antibodies

Table 2.6 Secondary antibodies

Conjugation	**Antigen**	**Host Species**	**Dilution**	**Catalog number**	**Provider**
Alexa Fluor 488	Goat IgG	Donkey	1:500	705-545-147	Jackson Immuno Research
Alexa Fluor 488	Rabbit IgG	Donkey	1:500	711-545-152	Jackson Immuno Research
Alexa Fluor 647	Rat IgG	Donkey	1:500	712-605-153	Jackson Immuno Research

Alexa Fluor 647	Rabbit IgG	Donkey	1:500	711-606-152	Jackson Immuno Research
Alexa Fluor 647	Goat IgG	Donkey	1:500	705-605-147	Jackson Immuno Research
Alexa Fluor 594	Rabbit IgG	Donkey	1:500	711-585-152	Jackson Immuno Research
Biotinylated	Rabbit IgG	Donkey	1:200	711-065-152	Jackson Immuno Research

2.7 Streptavidin-conjugates

Table 2.7 Streptavidin-Conjugates

Conjugation	**Dilution**	**Catalog number**	**Provider**
Alexa Fluro 488	1:500	016-540-084	Jackson Immuno Research
Alexa Fluro 594	1:500	016-580-084	Jackson Immuno Research
Alexa Fluro 647	1:500	016-600-084	Jackson Immuno Research

2.8 Software

Table 2.8 Software

Software	**Company**
Image J	NIH, Bethesda, MD, USA
GraphPad PRISM 7	Graph Pad Software Inc
Adobe Photoshop CC 2017	Adobe Systems Inc
LAS X software	Leica Microsystems
AngioTool	NIH, USA
EndNote X9	Thomson Reuters

3. Methods

3.1 Cell culture

Murine GBM cell lines GL261 and GL261-HSVTK-GFP were cultured in DMEM containing 10% fetal bovine serum, 1x MEM non-essential amino acids, and 1% penicillin-streptomycin. All cells were maintained at 37℃ in a humidified atmosphere of 95% O_2 and 5% CO_2.

3.2 Animal experiments

3.2.1 Animals

All animal experiments were performed in compliance with the German National Guidelines for Animal Protection and conducted with the approval of the local animal care committee of the Government of Oberbayern. Animals were kept in standard cages with access to water and food *ad libitum* in a 12h light/dark cycle at the Walter Brendel Center for Experimental Medicine, LMU Munich. Mice were sacrificed with symptoms or at defined points.

3.2.2 Tumor inoculation

Mice were anesthetized IP using a weight of 7uL/g of a mixture of 1.02 mL 10%

ketamine, 0.36 mL 2% Rompun and 4.86 ml 0.9% NaCl. A middle incision was made on the skin with a scalpel after disinfection with a 10% povidone iodine solution. To prevent the animals' corneas from drying out, their eyes were covered with Bepanthen cream. Mice were immobilized on a stereotactic frame in a flat-skull position. After drilling a hole into the skull with a 23G needle tip (coordinates 1.0 m anterior and 1.5mm right of the bregema), 1µl of cells (1×10^5 murine GBM cells/µl or 5×10^4 human GBM cells/µl in a supplement-free medium) was slowly injected within two minutes with a 22G Hamilton syringe at a depth of 3mm (the syringe was vertically inserted 4mm and retracted 1mm). Finally, the syringe was retracted 1mm/min, and the skin was carefully sutured.

3.2.3 Mice tail vein injection

Mice were anesthetized as previously described and placed in the restraining device. The tail was wiped with an alcohol-dampened gauze to disinfect the tail skin and increase vein visibility. The tail was immobilized using the non-dominant hand, and the needle was aligned parallel to the tail with the beveled edge of the needle. The needle was inserted into the tail vein starting from the distal end. When the injection was successful, blood flashed into the syringe and the injected materials flowed smoothly without resistance. If injection was not successful, a new position toward the base of the tail was chosen. The needle was removed after completing the administration, and the injection point was gently pressed with gauze (30–60 seconds) until bleeding

stopped.

3.2.4 Tamoxifen-inducible Cre-LoxP system

The Cre-LoxP system is a widely used technology for tracing cells to induce genetic modifications *in vivo*[113, 114]. The system consists of a single enzyme, Cre recombinase, which recombines a pair of short target sequences called the LoxP sequences. The gene Cre can be modified and fused with a mutant estrogen receptor (ER^{T2}), which acts as a tamoxifen specific receptor and does not bind natural estrogens or other physiological steroids[115]. In the absence of tamoxifen or hydro-tamoxifen, Cre-ER^{T2} protein is sequestered to the cytoplasm by heat shock protein 90[116], preventing nuclear recombination events. In transgenic mice that expressed Cre-LoxP in a defined cell population, tamoxifen injection enabled tracing of these cells or their progeny at desired times.

3.3 Single cell preparation

The tumor tissue was microdissected under a Leica M205 FA stereomicroscope. After washing with sterile 1X PBS, the tumor tissue was homogenated on ice using a mortar and pestle. Collagenase A (1mg/ml) and Dnase I (0.1mg/ml) were added and the sample was incubated for 10 minutes at 37℃. Following incubation, the tumor homogenate was centrifuged and the supernatant was discarded. The pellet was resuspended in sterile 1X PBS. Then the tissue homogenate was filtered through 40μm cell strainer. Discard

the filter and centrifuge the flowing solution. Discard the supernatant and re-suspend the pellet with FACS buffer.

3.4 Histology

3.4.1 Mice perfusion and brain tissue preparation

Mice were anesthetized with Nacoren® and intracardially perfused with 10ml 1X PBS, followed by a 15ml 4% paraformaldehyde (PFA) solution. The brain was carefully removed and incubated with 4% PFA at 4℃ for 24 hours and then immersed in 30% sucrose until the brain sank to the bottom of the tube. The brain was then embedded in Cryomatrix and frozen in 2,2,4-Trimethylpentane with liquid nitrogen. Sequential and horizontal 40μm-thick sections were prepared using a sliding microtome. Sections were stored in 24-well plates filled with cryoprotectant (ethylene glycol, glycerol, and 1X PBS with a ratio 1:1 ; two at pH 7.4) at -20℃ and protected from light.

3.4.2 H&E staining

H&E staining combined two histological stains (hematoxylin and eosin). Nuclei were stained blue by hematoxylin, and the cell cytoplasm was stained pink by eosin providing a clear view of the tissue structures. Staining was performed as follows: sections were: mounted on glass slides and air-dried for 15 minutes; dehydrated in 100% ethanol for 30 seconds; stained in a hematoxylin solution for two minutes;

rinsed in running water for five minutes; stained in 0.5% eosin for one minute and rinsed briefly in distilled water; dehydrated using a graded series of ethanol (70%, 96%, 100%) for one minute each time; cleared twice with xylene; and covered with an Entellan® mounting medium.

3.4.3 Tumor volume quantification

Tumor volume was quantified according to the Cavalieri principle. Every 12^{th} section was inspected under a microscope, and the tumor region was measured using the Axiovision Rel. 4.9 software. Stereotactical coordinates of mice brain sections were used to calculate the tumor Z-axis. Volume was calculated by multiplying the Z-axis with the average tumor area.

3.4.4 Quantification of tumor invasiveness

GBM cell invasion scores were calculated as previously described[117]. Every eighth tumor section was assigned an invasive score from 0 to 3 according to the following parameters: a score of 0 means no histological cell invasion from the tumor mass; a score of 1 represents a more extensive, connected group of invading GBM cells; a score of 2 describes smaller scattered groups of invading GBM cells; and a score of 3 indicates single, scattered, highly invasive GBM cells.

3.5 Immunofluorescence staining and quantification

3.5.1 Immunofluorescence staining of mouse brain sections

Floating sections were washed three times for five minutes in PBT (0.1% Tween-20 in 1X PBS) and then incubated in a blocking buffer (5% normal donkey serum and 0.3% Triton X-100 in 1X PBS) for one hour at room temperature. Samples were incubated with primary antibodies (Table 2.5) overnight at 4℃, washed with PBT three times for five minutes, and incubated with secondary antibodies (Table 2.6) for two hours at room temperature. All antibodies were diluted in a blocking buffer. Nuclei were stained with DAPI (1:10,000) for two minutes after washing three times in PBT. Finally, sections were mounted in a fluorescent mounting medium after washing.

3.5.2 Immunofluorescence staining for paraffin-embedded sections

Tissue sections were deparaffinized in ROTI® Histol for 20 minutes at room temperature. Slides were taken out and fixed in 70% acetone for 10 minutes at -20°C. After washing with PBT for five minutes three times, antigen retrieval was performed by immersing the sections in a citrate buffer and microwaving for 20 minutes. After slides cooled down, they were washed with PBT three times for five minutes, followed by blocking for 30 minutes (5% donkey serum and 0.3% Triton-X in 1× PBS). Sections were then incubated with goat anti-Sox2 (1:200) and rabbit anti-PU.1 (1:100) antibodies overnight at 4℃. The next day, sections were washed three times in PBT for five minutes and incubated with the secondary antibodies donkey anti-rabbit AF594

(1:200) and donkey anti-goat AF488 (1:200) for two hours at room temperature. All antibodies were diluted in a blocking buffer. Nuclei were stained with DAPI (1:10,000) for two minutes after washing three times in PBT. Finally, sections were mounted in Fluorescent Mounting Medium after washing.

3.5.3 Quantification of total vessel length

Mouse sections stained with CD31 were photographed to quantify vessel length and density within the tumor area. For each mouse, three or four sections with good quality containing a tumor were prepared, and nine 40X magnification images per section were taken using a TCS SP8 microscope. Vessel length density was analyzed using AngioTool 0.6 software.

3.6 Statistical analysis

All statistical analyses in this thesis were performed using GraphPad Prism 7 software. An unpaired Student's t-test was used when two independent groups were compared. The Log-rank (Mantel-Cox) test was used to determine statistical significance in survival experiments. The criteria for statistically significant differences was $p < 0.05$. P-values as shown in figures are: *, $p < 0.05$; **, $p < 0.01$; ***, $p < 0.001$; ****, $p < 0.0001$; and NS, not significant.

4. Results

4.1 Tracing a new myeloid-like cell population in glioblastoma

4.1.1 Using a Nestin-RFP mouse model to trace two RFP+ cell types in glioblastoma

The mouse model *Nestin*::CreER2:R26-RFP (abbreviated as Nes-RFP mice, Fig 4.1.1-A) allows tracing of nestin-expressing cells and their progeny in the glioblastoma microenvironment. Traced RFP+ cells were classified into two subgroups according to their position relative to tumor vessels (Fig 4.1.1-B). The first RFP+ subgroup (Fig 4.1.1-B, arrow), defined as vascular RFP+ cells, were close to blood vessels and wrapped around endothelial cells (Fig 4.1.1-B, CD31+ cells). Immunofluorescence staining for platelet-derived growth factor receptor B (PDGFRβ) identified vascular RFP+ cells as pericytes. The second RFP+ cell subgroup (Fig 4.1.1-B, arrowhead), defined as avascular RFP+ cells, did not show close contact with vessels and did not express PDGFRβ.

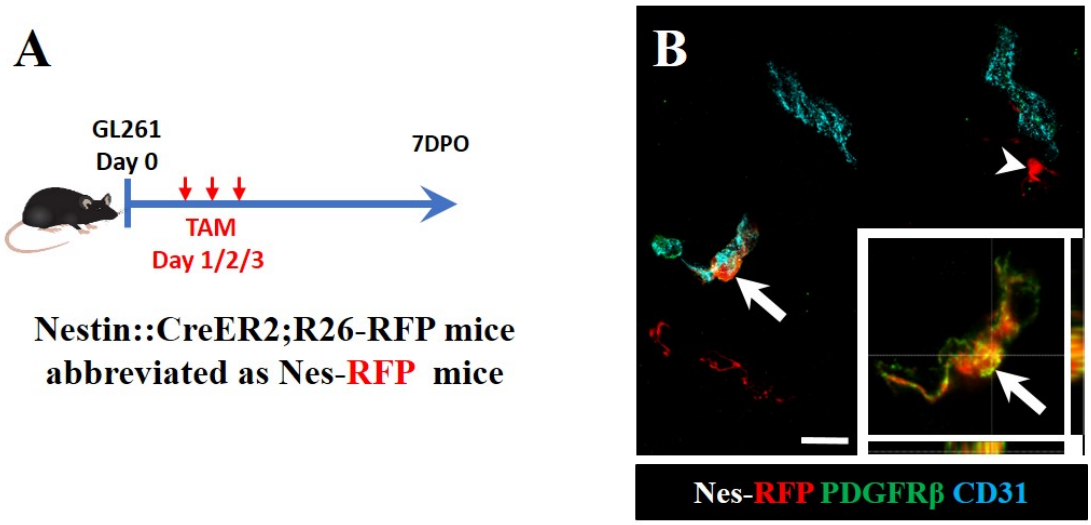

Figure 4.1.1 Traced vascular and avascular RFP+ cells in a Nes-RFP GBM mouse model. (A) Nes-RFP mice were inoculated with the murine GBM cell line GL261 at day 0. TAM was injected intraperitoneally at a dose of 75mg/kg at days 1, 2, and 3. Mice brains were harvested seven days post-operatively (DPO). **(B)** Immunofluorescence staining for PDGFβ (pericyte marker) and CD31 (endothelial cell marker) in 7DPO GBM tissue. Some RFP+ cells were located close to the vessel and were PDGFRβ positive (arrow) and one vascular RFP+ cell was PDGFRβ positive as shown in orthogonal view. Avascular RFP+ cells were PDGFRβ negative. The scale bar is 20 μm.

4.1.2 Avascular RFP+ cells have a myeloid-like expression profile

In order to uncover the avascular RFP+ cell-identity, tumors were dissected under a microscope at 7 and 21 days post-operatively (DPO, Fig 4.1.2-A). After tumor dissociation, avascular RFP+ cells were purified (Fig 4.1.2-B) and analyzed by single-cell RNA sequencing (scRNA-seq) [118]. Due to their tight association with tumor vessels, vascular RFP+ cells were removed during the isolation procedure (Fig 4.1.2-B)[119]. The isolated avascular RFP+ cells were compared with the expression profiles of over 3,000 neural and non-neural mouse cells [120] within the t-distributed stochastic neighbor embedding (t-SNE) plot, which demonstrated that they were a relatively homogeneous cell population (Fig 4.1.2-C) and that their expression profile was different from other known mouse brain cell populations. A random forest algorithm indicated that traced avascular RFP+ cells at 7 and 21DPO had a high statistical similarity to microglia (Fig 4.1.2-D).

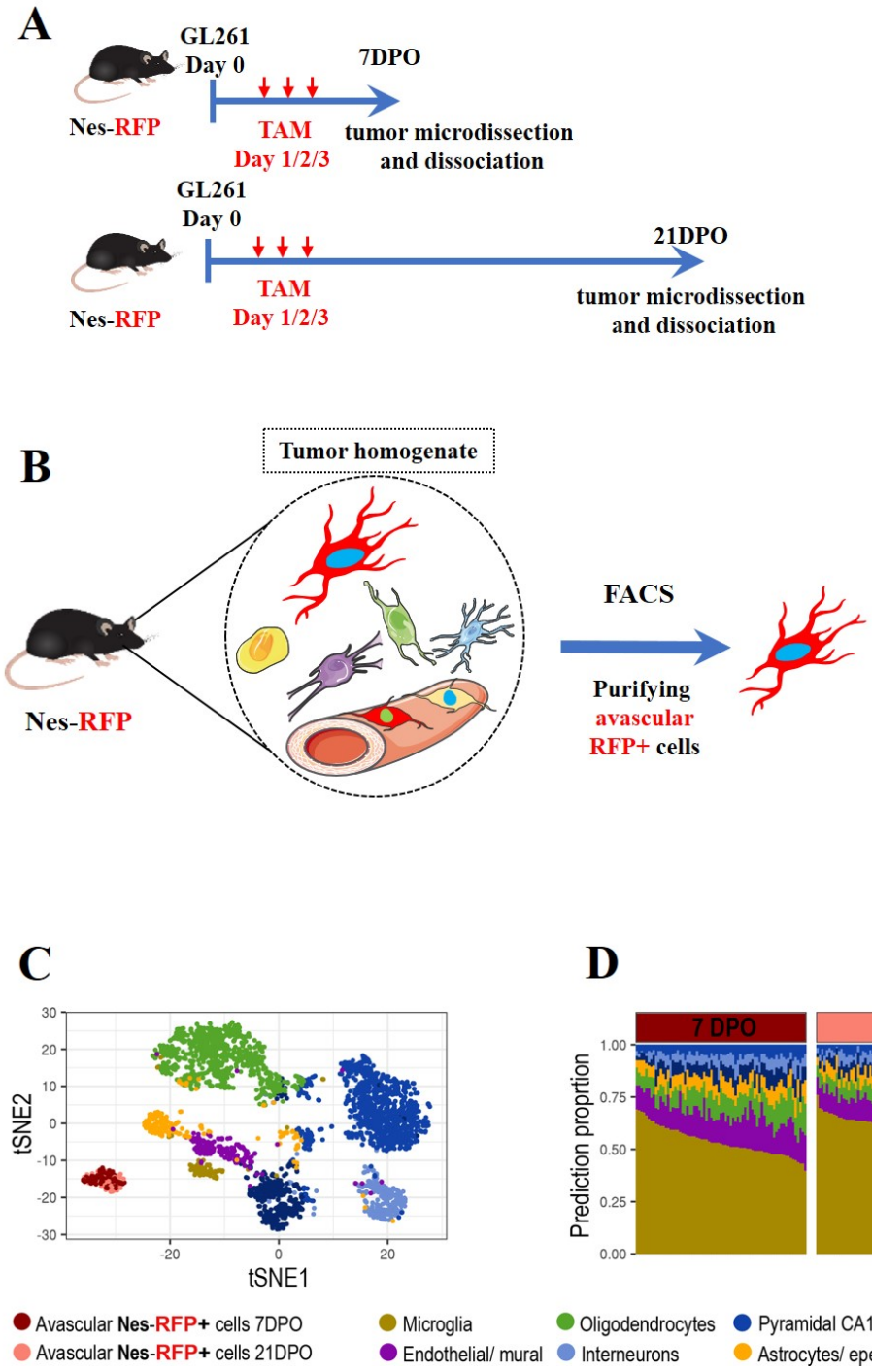

Figure 4.1.2 Purified avascular Nes-RFP+ cells from orthotopic GBM show a myeloid-like expression profile. (A) Experimental setup: 7DPO and 21DPO tumor tissues from Nes-RFP transgenic mice were microdissected and dissociated. **(B)** Scheme depicting avascular RFP+ cell purification. Microdissected tumor were triturated and subsequently digested into homogenate. Vascular RFP+ cells were

removed by filtering through 40µm cell strainer due to tight association with tumor vessels. The remaining avascular RFP+ cells were purified by fluorescence-activated cell sorting (FACS). **(C)** A t-SNE plot showed purified avascular RFP+ cells (red) with a scRNAseq analysis showing a distinct and homogenous cell population. **(D)** A random forest algorithm indicated a similar expression profile of 7DPO and 21DPO avascular RFP+ cells with microglia. The scRNAseq analysis was performed by Philipp Janssen, Wolfgang Enard, and Ines Hellmann (Anthropology and Human Genomics, Department Biology II, LMU Munich).

4.1.3 Characterization of traced avascular RFP+ cells

Tumor tissue of the 14DPO model was dissected under a microscope and dissociated (Fig 4.1.3-A). Vascular RFP+ cells, which are tightly conjugated with vessels, were excluded by filtering through 40µm cell strainer. Flow cytometry of traced avascular RFP+ cells indicated that they express the myeloid cell marker-CD11b (Fig 4.1.3-B). The *Spi1* gene encodes the transcription factor PU.1 and is required for both early differentiation and physiological function of mature myeloid cells and other lymphocytes[121]. We crossed the Nes-RFP mice and *Spi1*-GFP mice to characterize avascular RFP+ cells with a myeloid appearance and we found both markers colocalized in single, intratumoral cell (Fig 4.1.3-C). However, Iba1, a canonical marker of tumor- associated myeloid cells, was not detected in traced avascular RFP+ cells (Fig 4.1.3-D). SOX2 is a crucial stem cell transcription factor and plays an important role in differentiation of neural stem/precursor cells [122]. Immunofluorescence showed that while traced avascular RFP+ cells could express SOX2, vascular RFP+ cells do not (Fig 4.1.4-E). After conditionally knocking out gene

Sox2 in traced avascular RFP+ cells (*Nestin::*creER2, R26-RFP, $Sox2^{fl/fl}$), a much larger population of traced avascular RFP+ cells were reduced than only the population of initially characterized as SOX2-positive. Therefore, SOX2+ avascular RFP+ cells were the progenitor of traced avascular, myeloid-like cells and were necessary for maintaining the entire population of traced avascular cells [118]. Taken together, these results suggest that the traced avascular RFP+ cells constitute a previously unacknowledged cell population in the glioblastoma environment, with a myeloid-like expression profile (denominated: tumor-associated cells with a myeloid-like expression profile [TAMEP]).

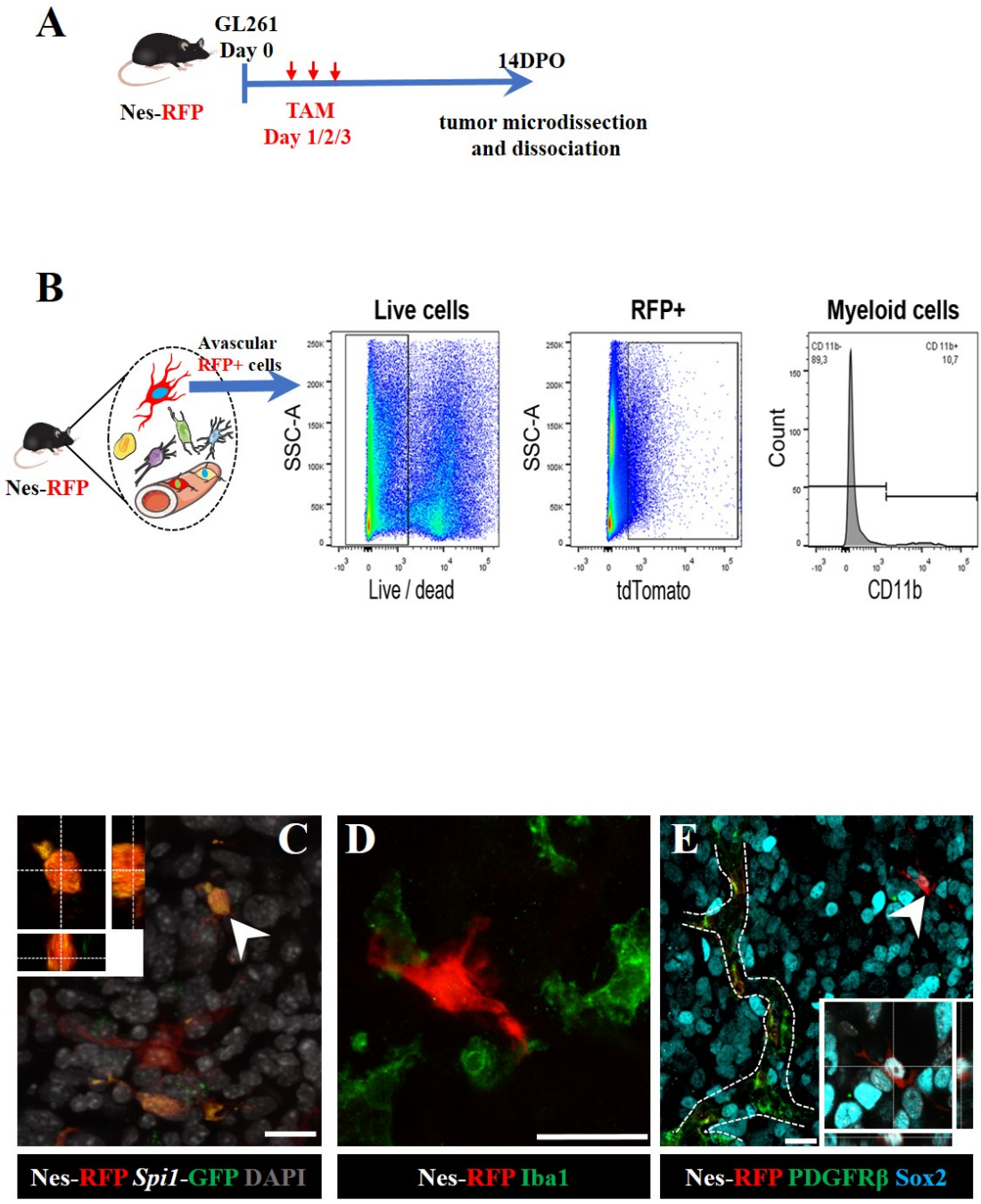

Figure 4.1.3 Characterization of traced avascular RFP+ cells. (A) Experimental setup: 14DPO Nes-RFP tumor tissue was microdissected and dissociated. **(B)** FACS analysis of the myeloid cell marker CD11b in avascular RFP+ cells from 14DPO tumor tissue (representative data of nine independent FACS experiments). **(C)** PU.1 transcription factor expression in avascular RFP+ cells taken from a Nes-RFP, *Spi1*-GFP glioma model (arrowhead points to a single cell is shown in orthogonal view). **(D)**

Immunofluorescence staining shows that Iba1 is not expressed in RFP+ cells from Nes-RFP tumor section. **(E)** SOX2 is expressed in avascular RFP+ cells (arrowhead, orthogonal view) but not in vascular RFP+ cells (the vessel is indicated by the dashed line). The scale bar is 20 μm.

4.1.4 TAMEP are not derived from microglia, macrophages, endothelial cells, or pericytes

The *Cx3cr1*::creER2, R26-RFP transgenic mouse strain is a useful model for tracing tumor-associated myeloid cells (TAMs) including CNS-resident microglia and peripheral macrophages [123]. Microglia can be specifically traced using tamoxifen pulse-chase protocols (abbreviated as CX3CR1-RFP Fig 4.1.4-A). Tumor cells were inoculated 4 weeks after tamoxifen injection, therefore RFP+ labelled peripheral macrophages disappeared before tumor inoculation due to the short half-life (2-3 weeks) of monocyte and monocyte-derived macrophages[124]. Immunofluorescence staining indicated that glioblastoma microglia do not express SOX2, suggesting that tumor-associated cells with a myeloid-like expression profile (TAMEP) do not originate from CNS-resident microglia (Fig 4.1.4-B). We injected TAMs at different time points to trace all TAMs including CNS-resident microglia and peripheral macrophages (Fig 4.1.4-C). SOX2 was also not expressed in the traced TAMs (Fig 4.1.4-D), indicating that TAMEP are also not derived from peripheral macrophages. Glioblastoma endothelial cells, marked in a *VE-cadherin*::creER2, R26-RFP mouse model [125], also did not express SOX2 (Fig 4.1.4-F), excluding them as a source for TAMEP.

The transgenic mouse model *PDGFRβ*::creER2, R26-RFP (abbreviated as PDGFRβ-

RFP) is widely used to trace pericytes[126]. Traced pericytes did not express SOX2 (Fig 4.1.4-H) or the myeloid cell markers PU.1 (Fig 4.1.4-I) and CD11b (Fig 4.1.4-J). These immunofluorescence results substantiated TAMEP was also not derived from pericytes.

We found that SOX2 plays an important role during TAMEP differentiation and maturation [118]. A conditional Sox2 knockout in traced avascular RFP+ cells caused a decrease in TAMEP cell number, thereby reducing GBM expansion [118]. We also investigated the effect of conditional Sox2 knockouts in microglia (*Cx3cr1*::creER2, R26-RFP, $Sox2^{fox/flox}$), endothelial cells (*VE-cadherin*::creER2, R26-RFP, $Sox2^{fox/flox}$), and pericytes (*PDGFRβ*::creER2, R26-RFP, $Sox2^{fox/flox}$) on GBM expansion. Conditional Sox2 knockouts in microglia, endothelial cells, and pericytes did not reduce tumor size relative to the control group ($Sox2^{WT/WT}$) (Fig 4.1.4-K).

Altogether, we used a range of transgenic mouse models to show that TAMEP are not derived from TAMs, endothelial cells, or pericytes.

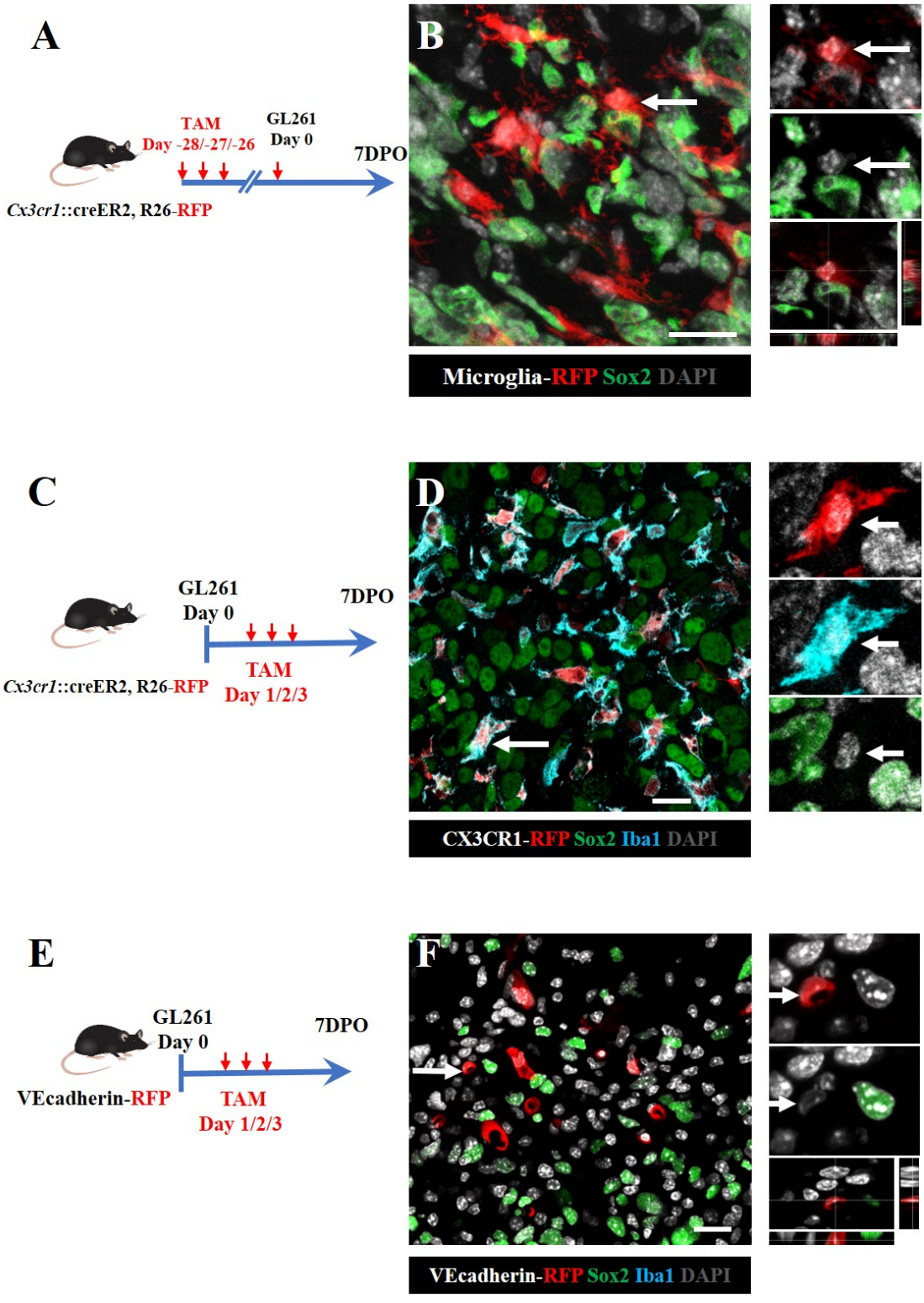

Figure 4.1.4 TAMEP are not derived from microglia, macrophages, endothelial cells, or pericytes. (A–B) A pulse-chase experiment in *Cx3cr1*::creER2, R26-RFP model was performed to trace microglia. TAM was given for three consecutive days.

Tumor cells were inoculated four weeks later after TAM injection and mice brain was harvested at 7DPO. In glioblastoma area, traced RFP+ cells were only microglia (RFP+ cells). SOX2 expression (green color) was not detected in traced glioma-associated microglia. Single traced microglia (red color) was SOX2 negative (arrow and orthogonal view). (**C–D)** Tumor cells were inoculated at day 0 and TAM were given at day 1/2/3. Traced RFP+ cells included all TAMs (CNS-microglia and peripheral macrophages)**.** In tumor area, SOX2 expression (green color) was not detected in all TAMs and all TAMs were Iba1 (cyan color) positive. The arrow indicated that a single traced RFP+ cell was Iba1 positive (cyan color) and SOX2 negative (green). **(E–F)** Tumor cells were inoculated at day 0 and TAM were given at day 1/2/3. Traced RFP+ cells were endothelial cells. SOX2 expression (green color) was not detected in endothelial cells. A single traced endothelial cell (red color) was SOX2 negative (arrow and orthogonal view).

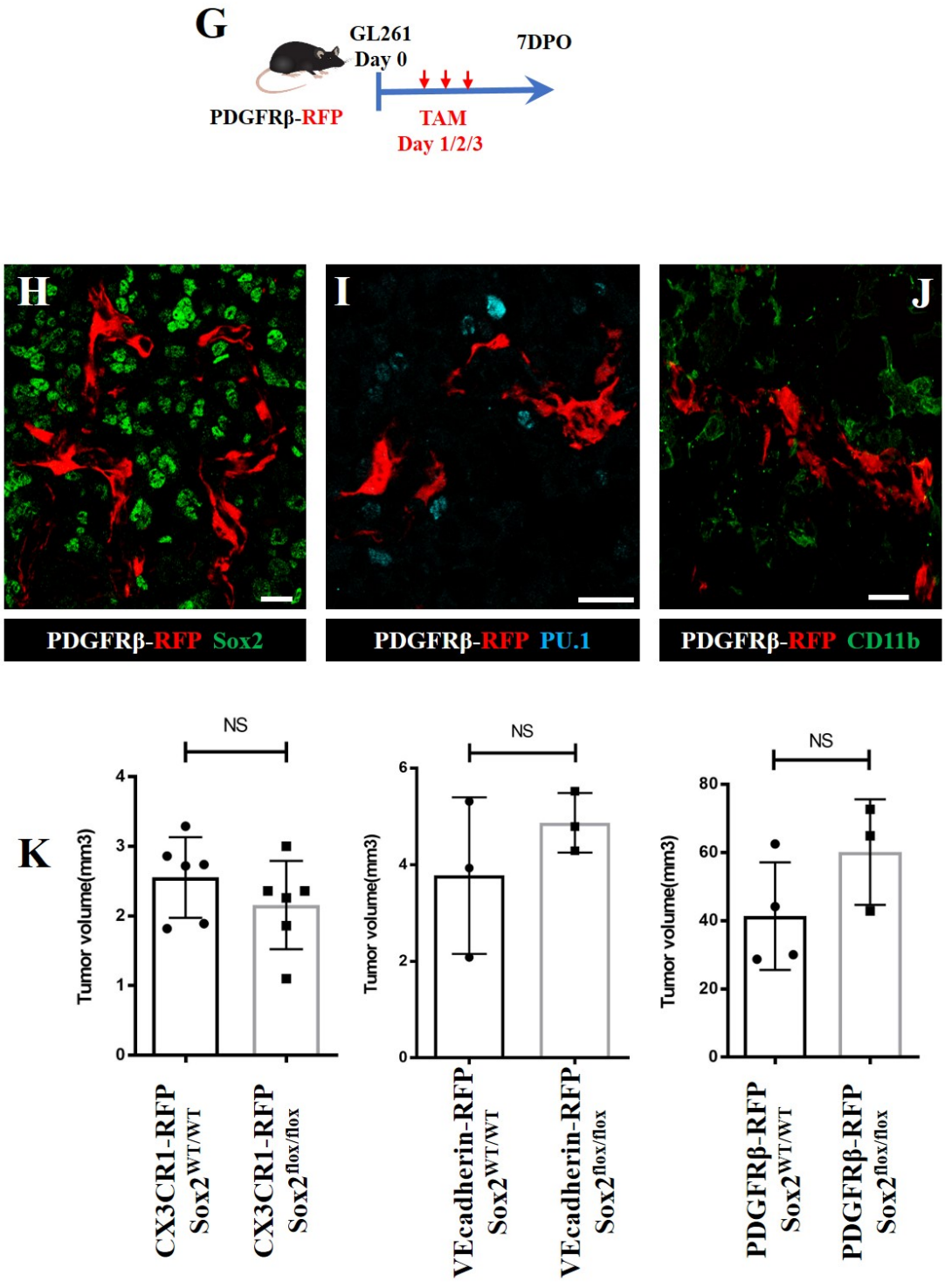

Figure 4.1.4 (G–J) Traced pericytes are SOX2 negative and do not express the myeloid cell markers PU.1 and CD11b. **(K)** Quantification of tumor size in the control group ($Sox2^{WT/WT}$) and conditional Sox2 knockouts in microglia (CX3CR1-RFP, $Sox2^{flox/flox}$), endothelial cells (VE-cadherin-RFP, $Sox2^{flox/flox}$), and pericytes (PDGFRβ::creER2,

R26-RFP, $Sox2^{fox/flox}$). Statistical significance was determined using a Student's t-test (NS representing no significant difference). Values are reported as the mean ± SEM. Each dot represents one mouse. The scale bar is 20 μm.

4.2 TAMEP are detected in additional GBM mouse model and human brain tumor tissue

4.2.1 Using the co-expression of SOX2 and PU.1 to identify TAMEP

By using the Nes-RFP transgenic mouse model and combining with different reporter mice for myeloid cells or with conditional alleles for *Sox2*-ablation, we found a previously unacknowledged cell population TAMEP in GBM environment, which was confirmed by experiments with lineage-tracing models indicating relevant cells of GBM microenvironment including microglia, macrophages endothelia or pericytes. Previous results showed TAMEP expresses both SOX2 and myeloid cell markers, including PU.1 (Fig 4.2.1-A). Therefore, we used the TAMEP-specific co-expression of SOX2 and PU.1 to extend our study to other models and human brain tumors. Since both SOX2 and PU.1 have a nuclear localization, immunohistochemistry and detection of SOX2/PU.1 can easily be used for cell identification. By crossing *Sox2*::IRES-creER2; R26-RFP mice (Sox2-RFP)[127] with *Cx3cr1*-GFP mice[128], we found that traced cells (SOX2 positive cells and progeny) had a myeloid appearance in glioblastoma (Fig 4.2.1-B). This result suggests that TAMEP are also identified by additional glioblastoma transgenic mouse model. Additionally, PU.1 was also expressed in the Sox2-traced cells (Fig 4.2.1-C), confirming SOX2 and PU.1 co-

expression in TAMEP. Based on these results, we suggest that combinatorial immunofluorescence detection of SOX2 and PU.1 is useful for identifying TAMEP in GBM mouse model and, possibly, also in human tissue, since co-expression of SOX2 and PU.1 has otherwise been reported only in some forms of leukemia[129].

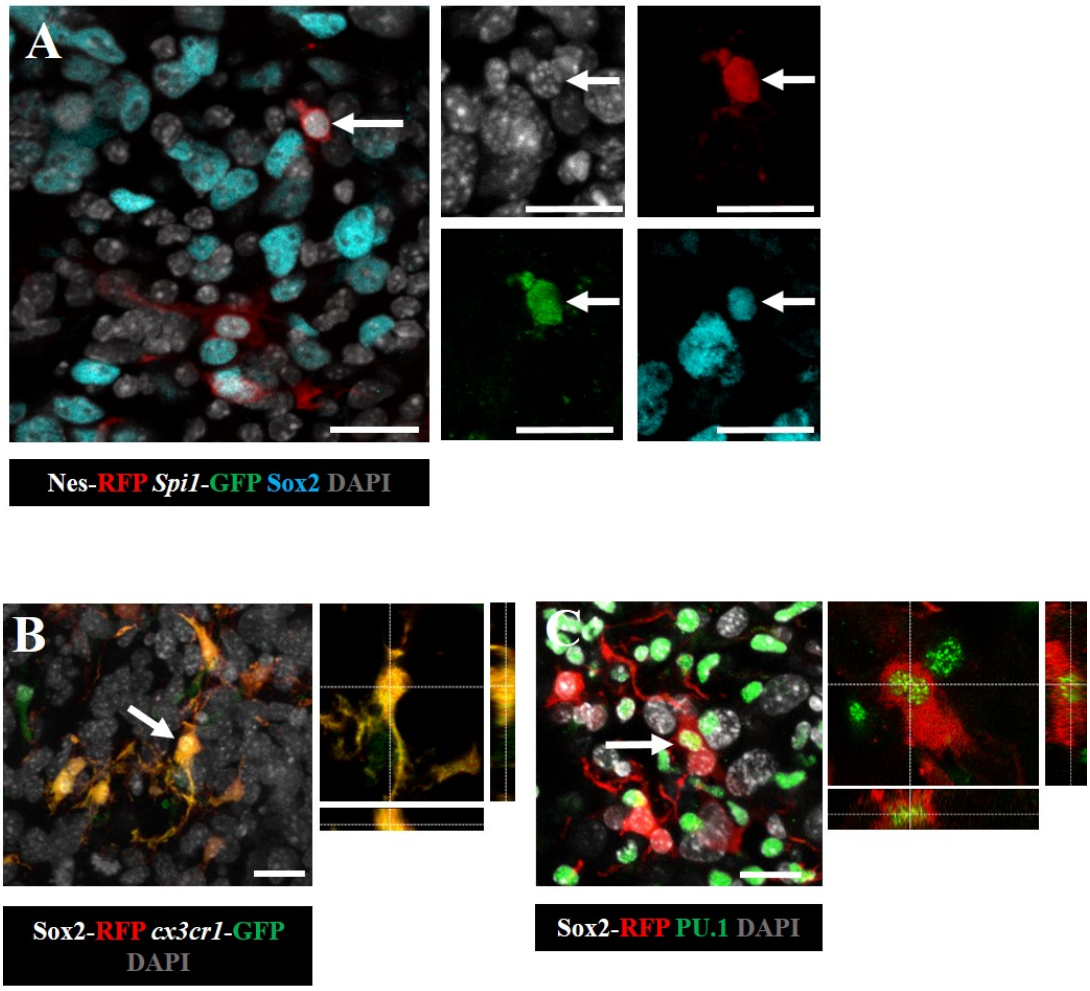

Figure 4.2.1 SOX2 and PU.1 are co-expressed in TAMEP. (A) SOX2 and GFP co-expression in traced avascular RFP+ cells in a Nes-RFP, *Spi1*-GFP glioma model. Arrow corresponds in single channel micrographs. Nuclei stained by DAPI are shown in grey. Immunofluorescence for SOX2 (cyan) in traced TAMEP (red and green). **(B)** *Sox2*::IRES-creER2, R26-RFP, *Cx3cr1*-GFP glioma model was used to trace TAMEP (red+ and green+; arrow). The orthogonal view showed single, magnified cell (arrow).

(C) Immunofluorescence staining of PU.1 (green) in traced cells (RFP+) in a *Sox2*::IRES-creER2, R26-RFP glioma model. The orthogonal view showed single, magnified cell (arrow). The scale bar is 20 μm.

4.2.2 TAMEP in genetically engineered GBM mouse models

We next turned to genetically engineered GBM mouse model for TAMEP identification. In this mouse model, subventricular zone (SVZ) stem cells of young cdkn2a-/- mice were transduced with the proto-oncogene *PDGFB* and transformed into GBM (Fig 4.2.2-A). Sox2 immunofluorescence staining was strong in the tumor area (Fig 4.2.2-B, dashed line) but not in the tumor-free, uninduced contralateral side (Fig 4.2.2-C). An abundance of TAMEP (Fig 4.2.2-D, arrowheads) was subject to regional heterogeneity in these experimental gliomas.

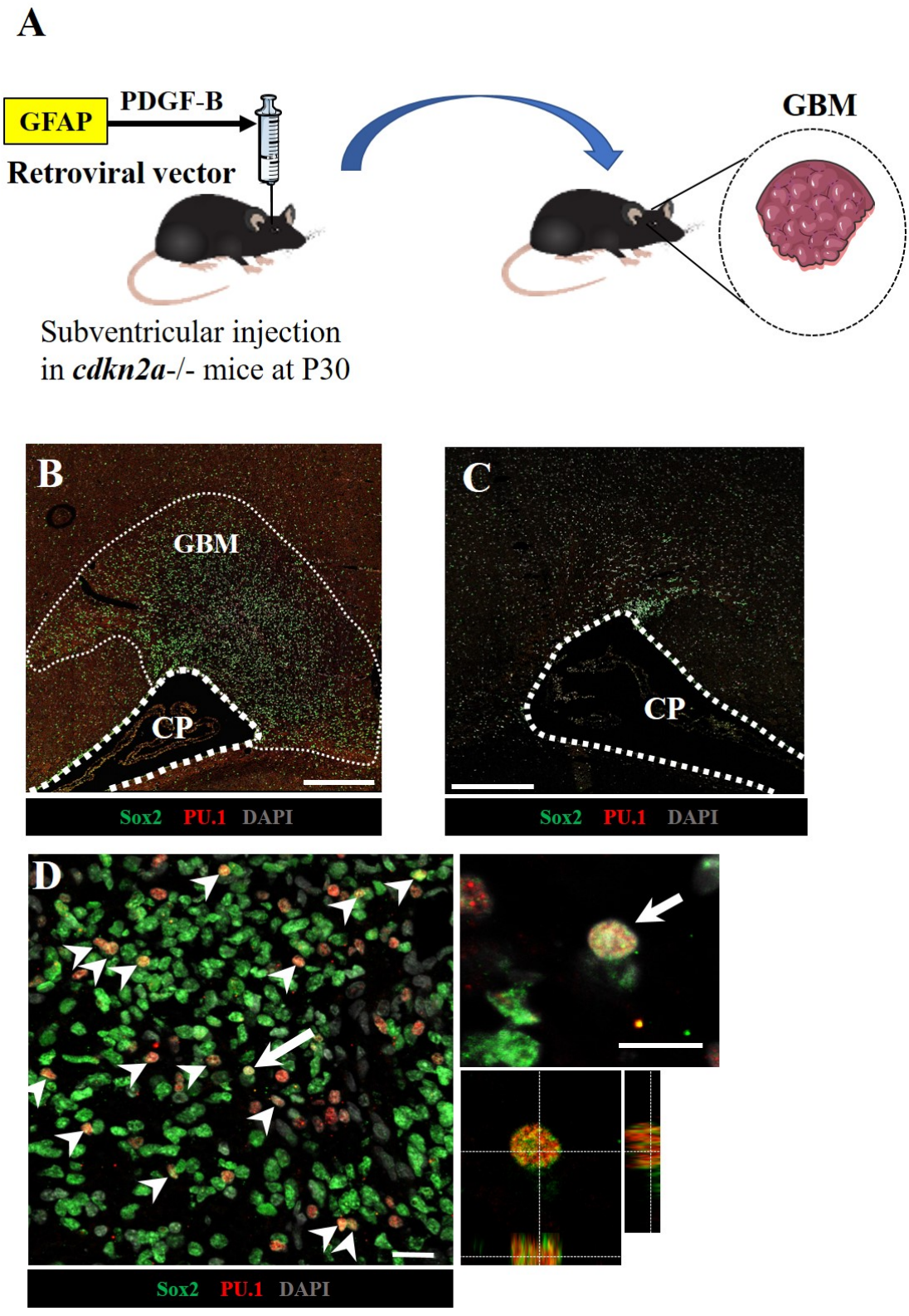

Figure 4.2.2 Tracing TAMEP in a genetically engineered GBM mouse model. (A) A retroviral vector containing the *PDGFB* gene, pseudotyped with a VSV-G envelope, was injected into the SVZ of young (postnatal day 30 [P30]) Cdkn2a-/- mice. PDGFB

expression was under glial fibrillary acidic protein (GFAP) promoter control. The SVZ transduced stem cells transform into GBM cells due to tumor suppressor gene *Cdkn2a* knockout and *PDGFB* upregulation. **(B–C)** Immunostaining for SOX2 (green) and PU.1 (red) in the tumor and contralateral sides. The GBM area (dashed line), lateral ventricle (dotted line), and choroid plexus (CP) are indicated. **(D)** Many TAMEP (SOX2+/PU.1+, arrowheads) were observed in the GBM area. The orthogonal view showed single, magnified TAMEP (arrow). The scale bars represent 400 μm (B–C), and 20 μm (D).

4.2.3 Human GBM tissue contains TAMEP

We also identified TAMEP in human primary and recurrent GBM tissue (Table 4.2). TAMEP (defined as SOX2 and PU.1 double-positive cells) were detected (Fig 4.2.3 A–E) in various primary GBM tissues; however, the amount of TAMEP varied. While some primary GBM tissues expressed a low amount of TAMEP per area (Fig 4.3.3 A–C), others exhibited high TAMEP levels (Fig 4.2.3 D–E). Even within the same GBM biopsy, we observed loco-regional heterogeneity of TAMEP density (Fig 4.2.3 E–F). In the recurrent GBM tissue, loco-regional heterogeneity of TAMEP was similar to that of primary GBM tissue. (Fig. 4.2.4 A–D).

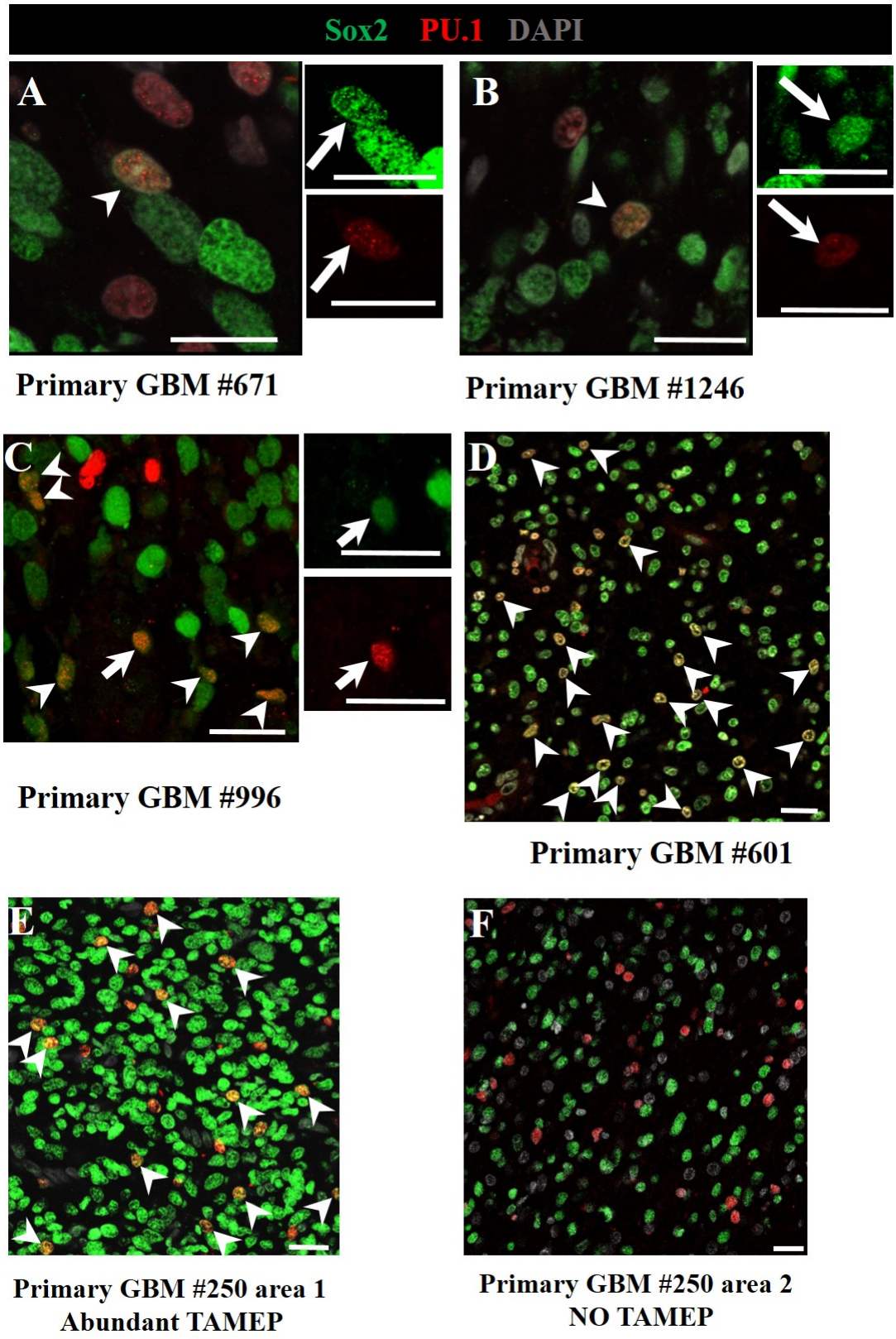

Figure 4.2.3 Detection of TAMEP in human primary GBM tissue. (A–B) Sox2 (green) and PU.1 (red) double-labeled cells in primary GBM tissue #671 and # 1246.

Only one TAMEP was detected per tumor area (arrowhead indicates TAMEP, arrow corresponds in single channel micrographs). **(C–D)** Sox2 (green) and PU.1 (red) double-labeled cells in primary GBM tissue #996 and #601. TAMEP were abundant per tumor area (arrowheads indicates TAMEP, arrow corresponds in single channel micrographs). **(E-F)** In primary GBM tissue #250, loco-regional heterogeneity of TAMEP density was observed. Many TAMEP (arrowheads) were detected in area 1. However, TAMEP were not detected in area 2. The scale bar is 20 µm.

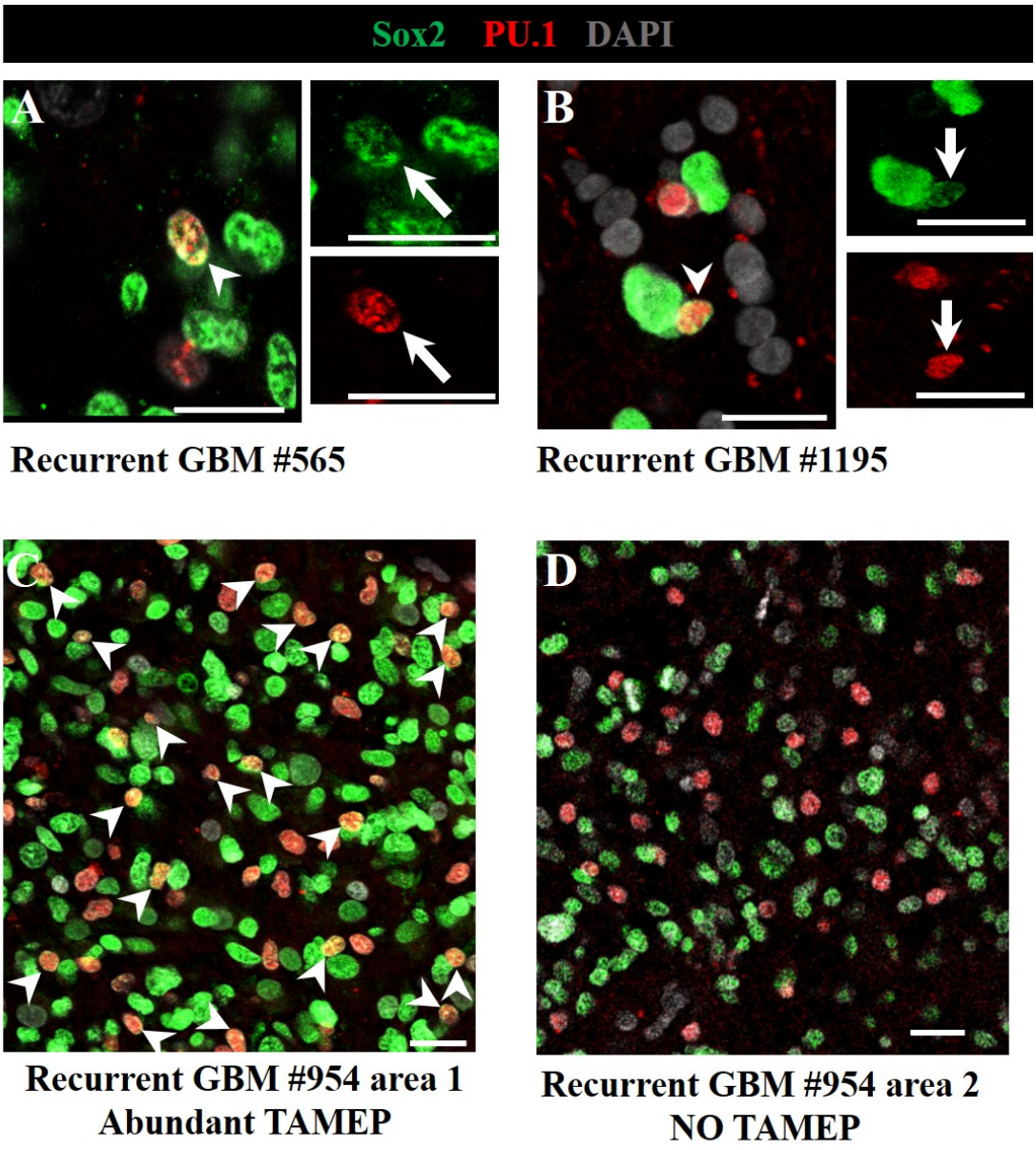

Figure 4.2.4 Detection of TAMEP in human recurrent GBM tissue. (A–B) Sox2 (green) and PU.1 (red) double-labeled cells in recurrent GBM tissue #565 and # 1195. Only one TAMEP was detected per tumor area (arrowhead indicates TAMEP, arrow corresponds in single channel micrographs). **(C–D)** In recurrent GBM tissue #954, loco-regional heterogeneity of TAMEP density was observed. Many TAMEP (arrowheads) were detected in area 1. However, TAMEP were not detected in area 2. The scale bar is 20 μm.

4.2.4 TAMEP can be detected in other brain tumor types

Since TAMEP were detected in human GBM tissue, we sought to determine whether TAMEP existed in other human brain tumor tissue (Table 4.2). We stained the human brain tumor tissue array (human brain tumor tissue from different patients in one slide) for SOX2 and PU.1. SOX2/PU.1 double-positive cells were detected in low-grade glioma (Fig 4.2.4-A), medulloblastoma (Fig 4.2.4-B), and in metastatic brain tumors (Fig 4.2.4-C). We also observed areas with abundant TAMEP in metastatic brain tumors (Fig 4.2.-C).

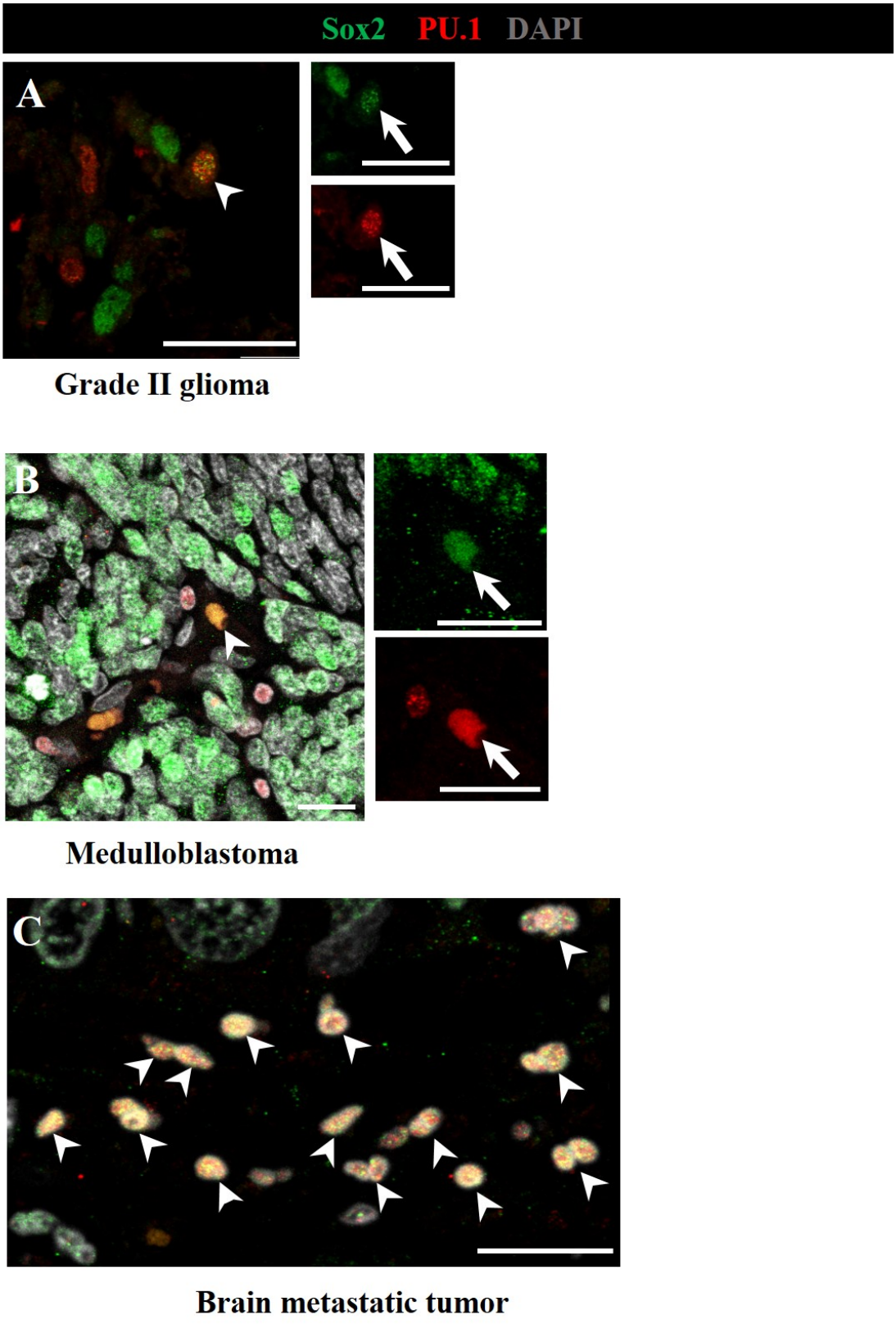

Figure 4.2.5 Detection of TAMEP in a human brain tissue array. Sox2 and PU.1 double-labeled cells in **(A)** Grade II glioma (arrowhead indicates SOX2/PU.1 double-

labeled cells, arrow corresponds in single channel micrographs), **(B)** medulloblastoma (arrowhead indicates SOX2/PU.1 double-labeled cells, arrow corresponds in single channel micrographs) and, **(C)** brain metastatic tumor (arrowhead indicates SOX2/PU.1 double-labeled cells). The scale bar is 20 μm.

Table 4.2 Human brain biopsies

Patient tissue number	Diagnosis	Gender	Age	TAMEP detected
9	Primary GBM	M	50	Yes
1028	Primary GBM	M	38	Yes
1235	Primary GBM	M	63	Yes
1074	Primary GBM	M	65	Yes
1246	Primary GBM	M	30	Yes
671	Primary GBM	M	44	Yes
374	Primary GBM	F	71	Yes
717	Primary GBM	M	67	Yes
703	Primary GBM	M	42	Yes
601	Primary GBM	F	55	Yes
250	Primary GBM	F	63	Yes
1195	Recurrent GBM	M	68	Yes
1200	Recurrent GBM	M	41	Yes
508	Recurrent GBM	M	31	Yes
954	Recurrent GBM	M	45	Yes
565	Recurrent GBM	F	72	Yes
421	Recurrent GBM	M	44	Yes
BC17012c-C7	Medulloblastoma	M	34	Yes
GL861-C8	Brain metastasis	F	58	Yes
GL861-E10	Brain metastasis	F	51	Yes
BC17012c-G7	cerebrum	M	35	No
BC17012c-G8	cerebrum	M	48	No
BC17012c-G9	cerebrum	F	24	No
BS17016c-H1	Tumor-adjacent normal brain tissue	F	8	No
BS17016c-H3	Tumor-adjacent normal brain tissue	M	30	No
BS17016c-H6	Tumor-adjacent normal brain tissue	M	38	No

4.3 Establishing a novel recurrent GBM mouse model

4.3.1 Ganciclovir induces GL261-HSVTK-GFP cell death

Since TAMEP were detected in human primary and recurrent GBM tissue. We aim to establish a recurrent GBM mouse model to explore the role of TAMEP in recurrent GBM.

Ganciclovir (GCV) application can induce cell death in a GL261 cell line transfected with the herpes simplex virus thymidine kinase (HSVTK) by inhibiting DNA synthesis (Fig 4.3.1-A). In mouse GBM model, resection of tumor at pathologically relevant location, for example in striatum, could not be accessed surgically. So we used this HSVTK/GCV system to eliminate the tumor mass and establish a new mouse model to investigate recurrent GBM. Experiments were performed according to the experimental setup in Figure 4.3.1 A. Firstly, GL261-HSVTK-GFP cells were inoculated into mice brain to induce orthotopic glioma. At 14DPO, mice brain will be harvested to verify the tumor has grown. Next, ganciclovir was injected intraperitoneally at 14-17 DPO after tumor grew two weeks. GCV application could reduce tumor mass by inducing tumor cell death through activating the HSVTK/GCV system. At 21DPO, mice brain were harvested and histopathological inspection verified that tumor mass was largely reduced. However, some residual tumor cells continued to grow, leading to GBM recurrence. The mice brain were harvested to verify that GBM has recurred when mice are symptomatic.

To test the HSVTK/GCV system's efficiency, we first conducted an *in vitro* experiment. The transgenic glioma cells (GL261-HSVTK-GFP) were cultured in 24-well plates. In the experiment group, ganciclovir was applied. And the same volume PBS was added into control group. GCV-treated cells died rapidly, while cells in control group proliferated (Fig 4.3.1-B). The result showed GCV could induce GL261-HSVTK-GFP cells death efficiently.

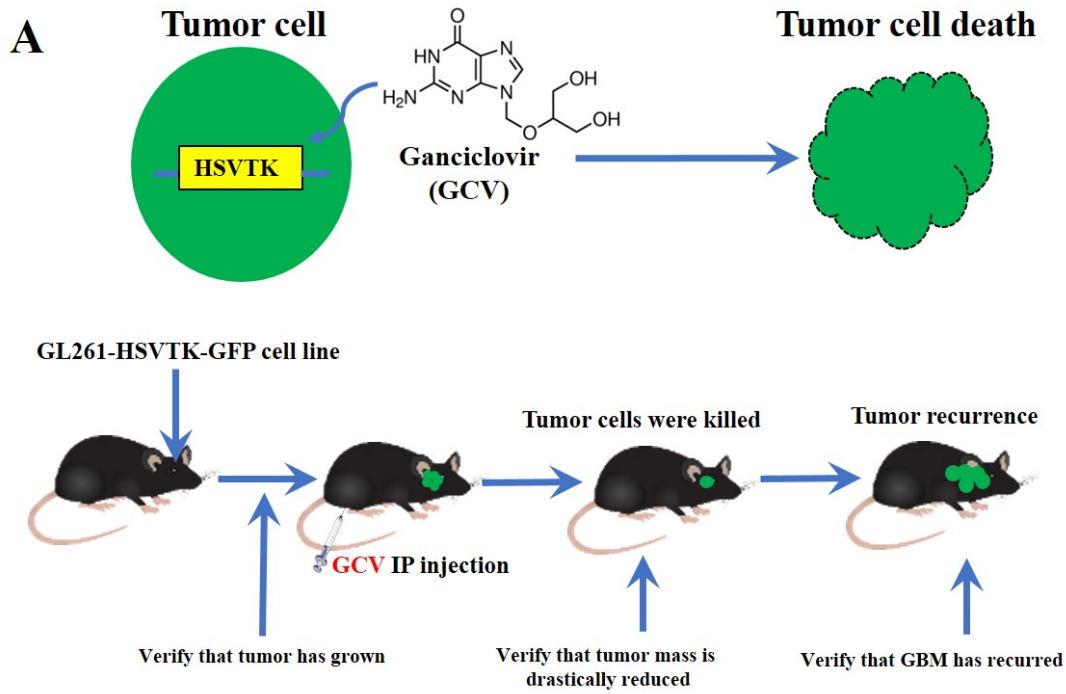

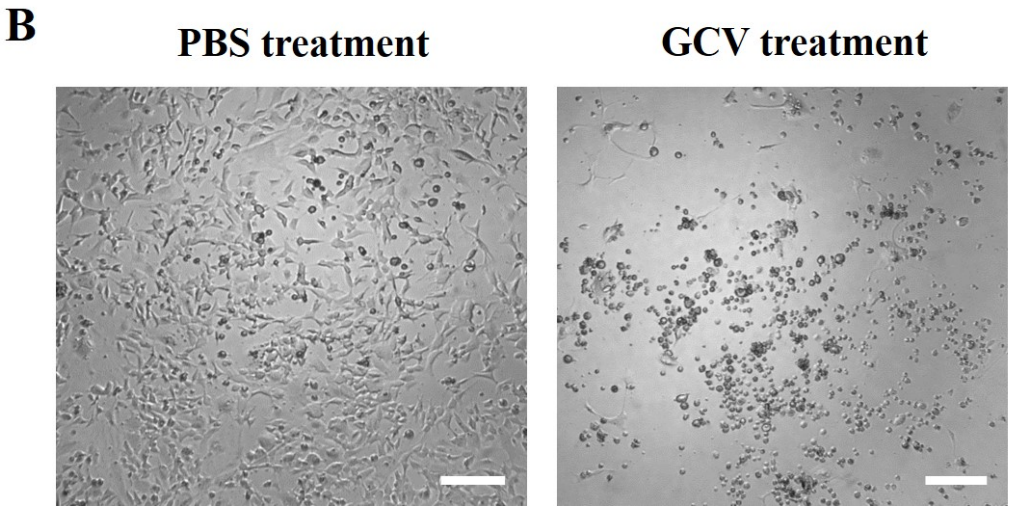

Figure 4.3.1 Schematic diagram of the recurrent GBM model and the HSVTK/GCV system test in *vitro*. (A) HSVTK expression causes cells to phosphorylate GCV, which interferes with DNA replication and induces apoptosis. GL261-HSVTK-GFP cells were inoculated into mice brain to induce orthotopic GBM.

Tumor growth was verified before GCV injection. GCV was injected intraperitoneally during tumor growth, which largely eliminated the tumor. Mice brain were harvested to verify that tumor mass is reduced. Some residual cells escaped the ganciclovir induced cell-ablation and eventually caused tumor recurrence. Mice brain were harvested to verify tumor has recurred when mice are symptomatic. **(B)** Representative microscopy images for the *in vitro* HSVTK/GCV experiment. The **s**cale bar is 200 μm.

4.3.2 Ganciclovir strongly reduces tumor size and prolongs survival in the tumor-relapse model

We next investigated the effect of the HSVTK/GCV system *in vivo* according to the setup presented in Fig 4.3.2-A. In the experimental group, GCV (50mg/kg) was injected intraperitoneally at day 14, 15, 16 and 17. In the control group, GL261-HSVTK-GFP cells were inoculated and GCV was not injected. Mice were sacrificed at 21DPO and separated into two groups. In experimental group, tumor size was significantly decreased at 21DPO compared to the control group (Fig 4.3.2-B). Next, we analyzed mouse survival after GCV injection (experimental setup in Fig 4.3.2-C). Mice were sacrificed when symptoms manifested, and the cumulative survival was recorded. The control group's median survival was 21 days, while mice treated with GCV survived longer, with a median survival of 55 days (Fig 4.3.2-D).

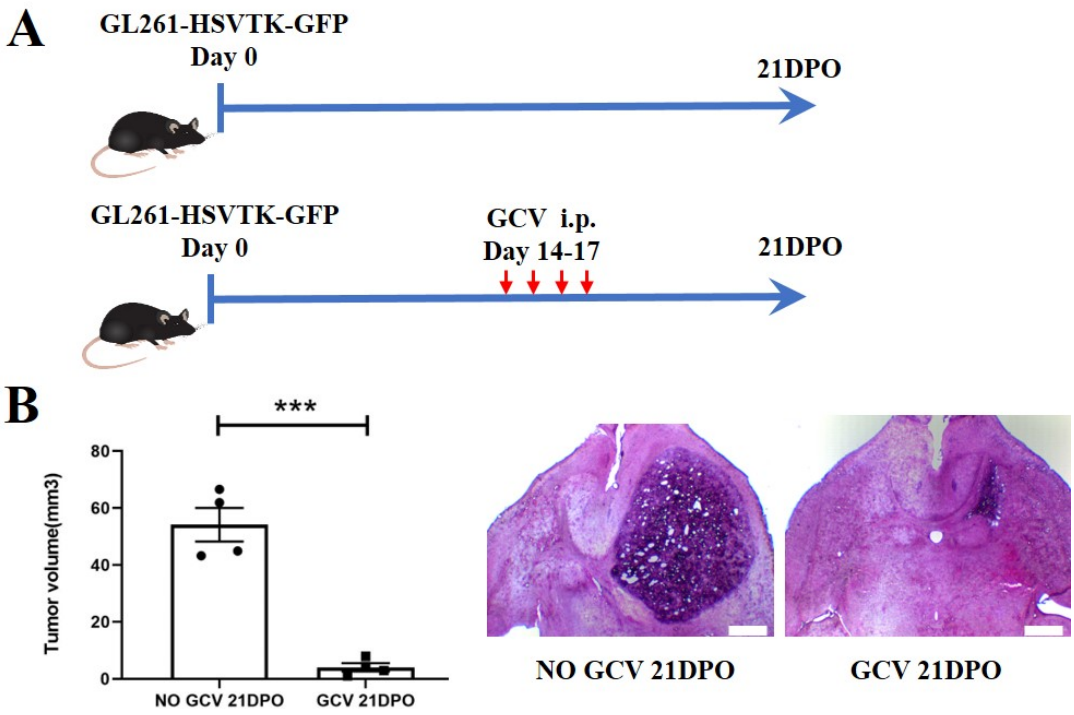
A
GL261-HSVTK-GFP
Day 0
21DPO
GL261-HSVTK-GFP
Day 0
GCV i.p.
Day 14-17
21DPO
B
***
Tumor volume(mm3)
80
60
40
20
0
NO GCV 21DPO
GCV 21DPO
NO GCV 21DPO
GCV 21DPO

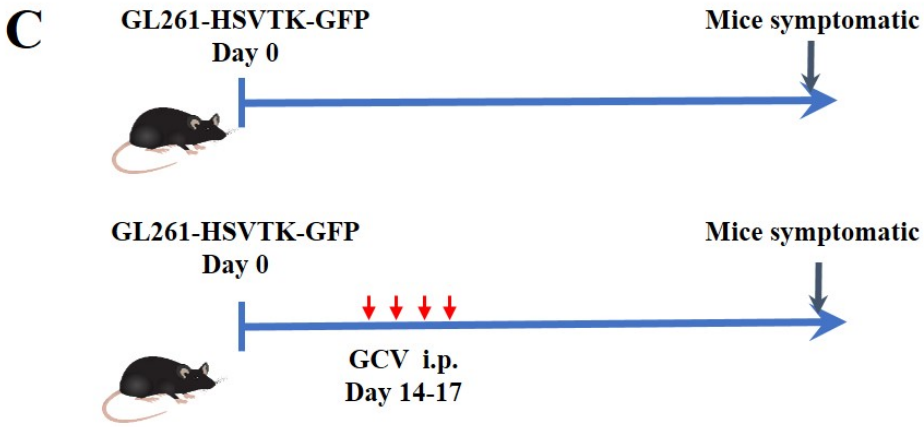
C
GL261-HSVTK-GFP
Day 0
Mice symptomatic
GL261-HSVTK-GFP
Day 0
Mice symptomatic
GCV i.p.
Day 14-17

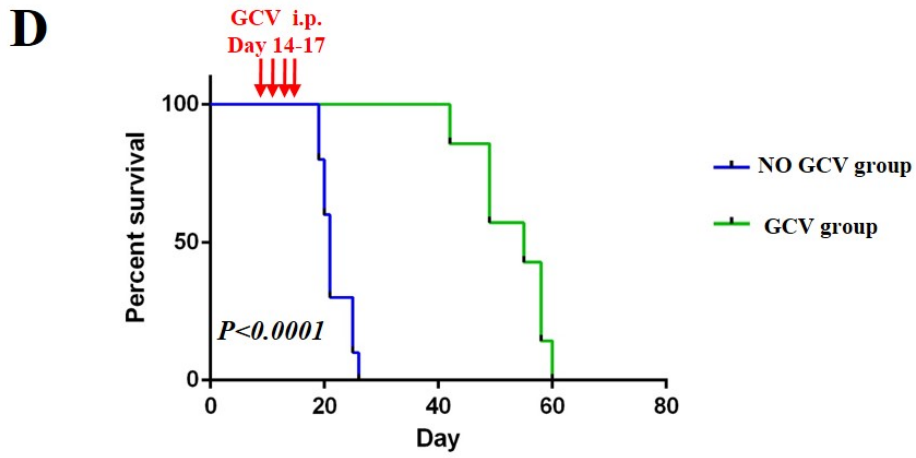
D
GCV i.p.
Day 14-17
Percent survival
100
50
0
P<0.0001
0
20
40
60
80
Day
NO GCV group
GCV group

Figure 4.3.2 HSVTK/GCV system *in vivo*. (A) A schematic diagram depicting the GCV application *in vivo*. GCV (50mg/kg) was injected at days 14–17 and mice were sacrificed 21DPO. **(B)** Quantification of tumor volume and representative microscopy images of the control and GCV-treated groups, showing a significant difference between the two groups. **(C–D)** Schedule of GCV application in the survival experiment. GCV (50mg/kg) was injected at days 14–17 and mice were sacrificed once they became symptomatic. The median survival time was 21 days in the control group (n=10) and 55 days in the GCV-treated group (n=7). Statistical significances were calculated using a Student's t-test (B) or a Log-rank (Mantel-Cox) test (D), *** $p < 0.005$. Values (B) are reported as the mean ± SEM. Each dot represents one mouse. The scale bar is 1mm.

4.3.3 Tumor recurrence after GCV application

In order to observe how GCV-treatment affects GBM growth after treatment, tumor size was quantified at different time points (21 DPO, 28 DPO, 35-42 DPO, mice symptomatic) following GCV injections (at day 14, 15, 16, and 17) according to the experimental setup in Fig 4.3.3-A. The GCV injection lasted four days in total and the effect of GCV-induced tumor cell death was sustained for nearly two weeks. GCV decreased tumor volume up to 28DPO (Fig 4.3.3-B), after which the tumor began to regrow. Our model recapitulated the initial tumor growth, therapeutic reduction of tumor mass and subsequent tumor regrowth that is characterized for GBM-relapse.

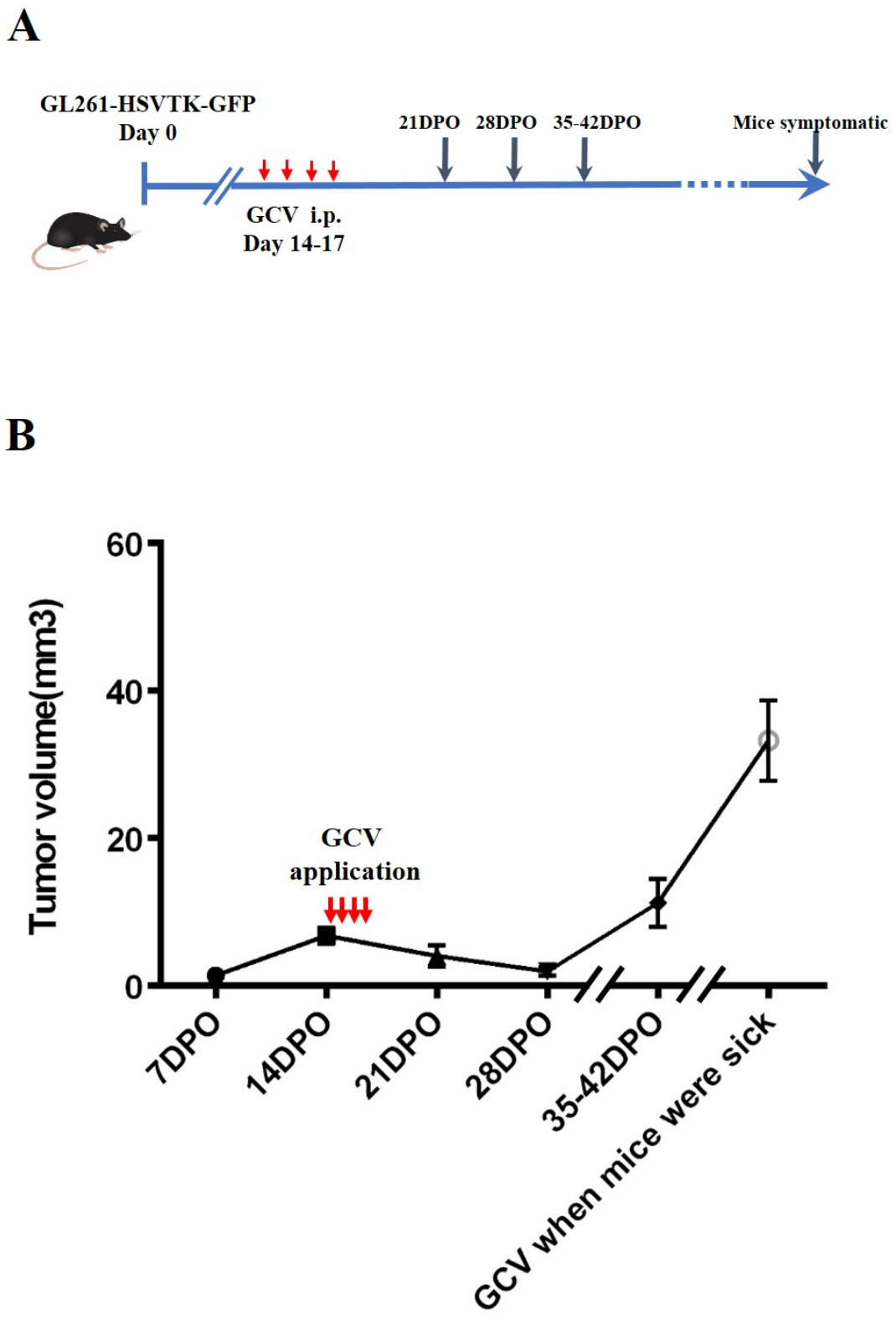

Figure 4.3.3 Observation of tumor volume changes after GCV application. (A) Schematic diagram of the experimental setup in which tumor volume was measured at different time points. **(B)** Quantification of the tumor volume. Tumor volume was

quantified at 7 (n=6), 14 (n=6), 21 (n=4), 28 (n=4), 35-42 (n=6) DPO and humane endpoint (n=7).

4.4 Characterization of recurrent glioblastoma in a mouse model

4.4.1 Recurrent GBM are more invasive than primary GBM

In the GCV-treated mice, GBM recurred at both the original tumor site (Fig 4.4.1 A and C, arrowhead) and in other locations (Fig 4.4.1 A and C, arrow). This distant recurrence indicates that the GCV-treated GBM cells became much more invasive than the primary tumor.

We assessed the extent of the GCV-treated GBM invasion by scoring the degree of invasiveness on a scale of 0–3 (0 represents no histological invasion, 1 shows the appearance of a larger and connected group of tumor cells, 2 describes smaller scatted groups of invading tumor cells, and 3 indicates single scattered highly invasive tumor cells). In the primary GBM mouse model, 7DPO, 14DPO, and 21DPO tumors (mice usually get symptomatic around 21DPO) represent early, intermediate, and late tumor growth periods, respectively. The adjusted time points in the recurrent GBM group were determined according to tumor size and were set at 28DPO, 35DPO, and at symptom appearance. In the early tumor growth period, there is no difference in tumor volume between untreated 7DPO and GCV 28 DPO (1.70 VS 1.42, Fig 4.4.1 E). However, the invasive score was significantly higher in GCV treated mice (1.86 VS 0.97, Fig 4.4.1 E). In the intermediate tumor growth period, untreated 14DPO and GCV 35DPO tumor volume were similar (6.45 VS 7.95, Fig 4.4.1 F). The invasive score of recurrent GBM

was also significantly higher than that of primary GBM in intermediate tumor growth stage (1.54 VS 1.12, Fig 4.4.1 F). Although the recurrent tumor size was smaller than the primary GBM (27.47 VS 54.47, Fig 4.4.1 G) in the late tumor growth period, the invasive score of recurrent GBM was still significantly higher than that of primary GBM (1.74 VS 1.12, Fig 4.4.1 G).

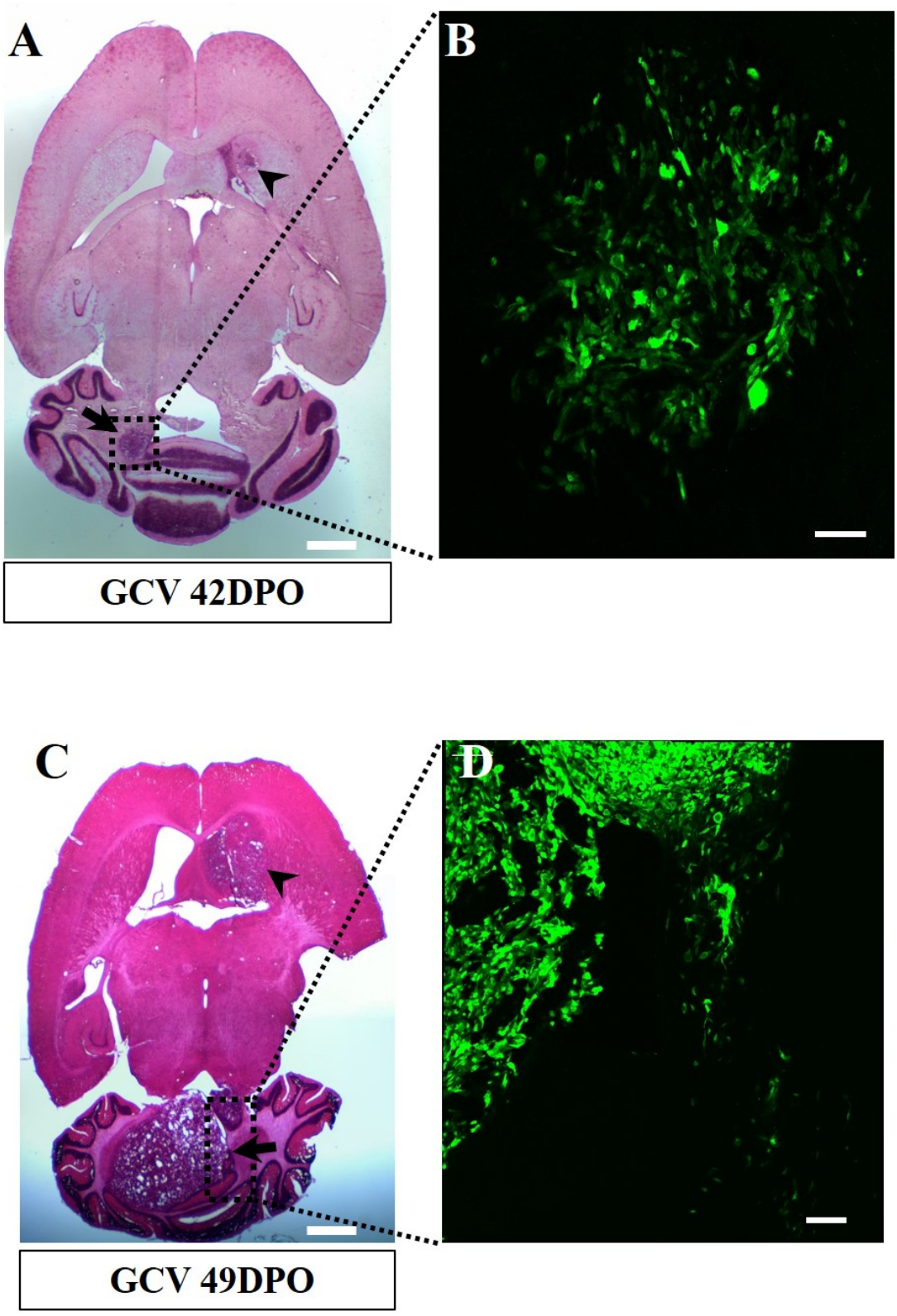

Figure 4.4.1 Increased invasiveness in GCV-treated tumor cells compared to untreated tumor cells. (A, C) GBM recurred at both original sites and distant locations. Hematoxylin and Eosin staining (H&E staining) show local (arrowheads) and distal

tumor recurrence (arrows). Distant recurrence (circled by dashed line) was confirmed by GFP immunofluorescence. The scale bars are 1mm in A and C, 100 μm in B and D.

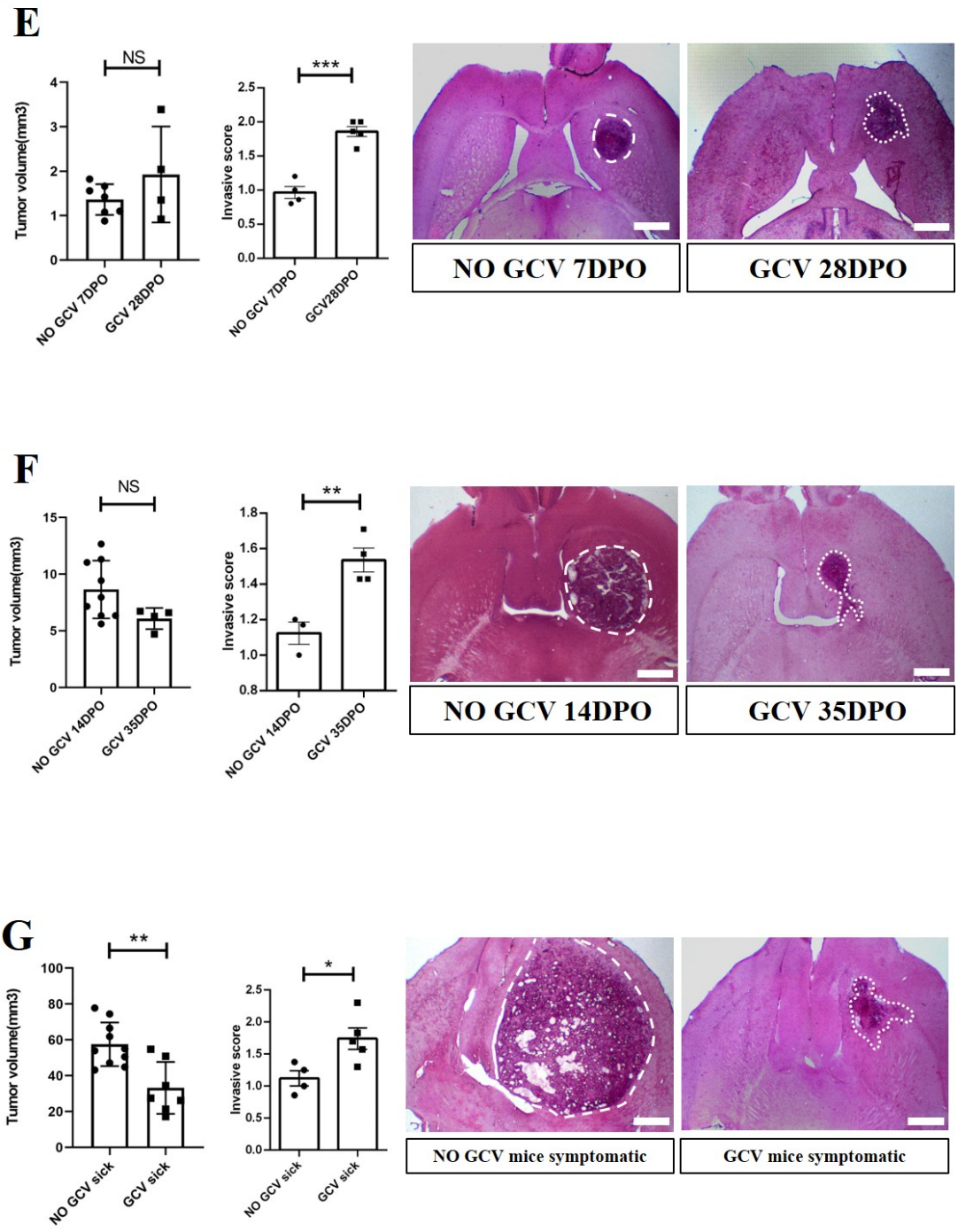

Figure 4.4.1 (E) In the early tumor growth stage. There is no difference in tumor size between NO GCV 7DPO and GCV 28DPO. However, the invasive score is much higher

in GCV 28DPO than NO GCV 7DPO. **(F)** In the intermediate tumor growth stage. There is no difference in tumor size between NO GCV 14DPO and GCV 35DPO. The invasive score is higher in GCV 35DPO than NO GCV 14DPO. **(G)** In recurrent symptomatic mice as compared to primary tumor, the main tumor mass is smaller but the invasive score remains higher at the "humane endpoint" (when mice are symptomatic). Representative images of HE staining showed defined tumor borders in primary GBM (dashed line) and irregular, infiltrative edges (dotted line) in recurrent GBM. Statistical significance was calculated according to a Student's t-test, * $p < 0.05$, ** $p < 0.01$, *** $p < 0.0005$. Each dot represents one mouse. Values are reported as the mean ± SEM. The scale bars are 1 mm in (A), (C), (E–G), 100 μm in (B) and (D).

4.4.2 Recurrent GBM is less angiogenic than primary GBM

Angiogenesis levels in primary and recurrent GBM were evaluated by immunostaining for CD31 (Fig 4.4.2 A–C). Total vessel length was measured in treated and untreated groups at different time points (as selected according to tumor growth, see the previous section). In the tumor's early, intermediate and late stages, the total vessel length in recurrent GBM was significantly decreased compared to the corresponding stage in primary GBM (Fig 4.4.2 A–C), suggesting that recurrent GBM tumors are less angiogenic.

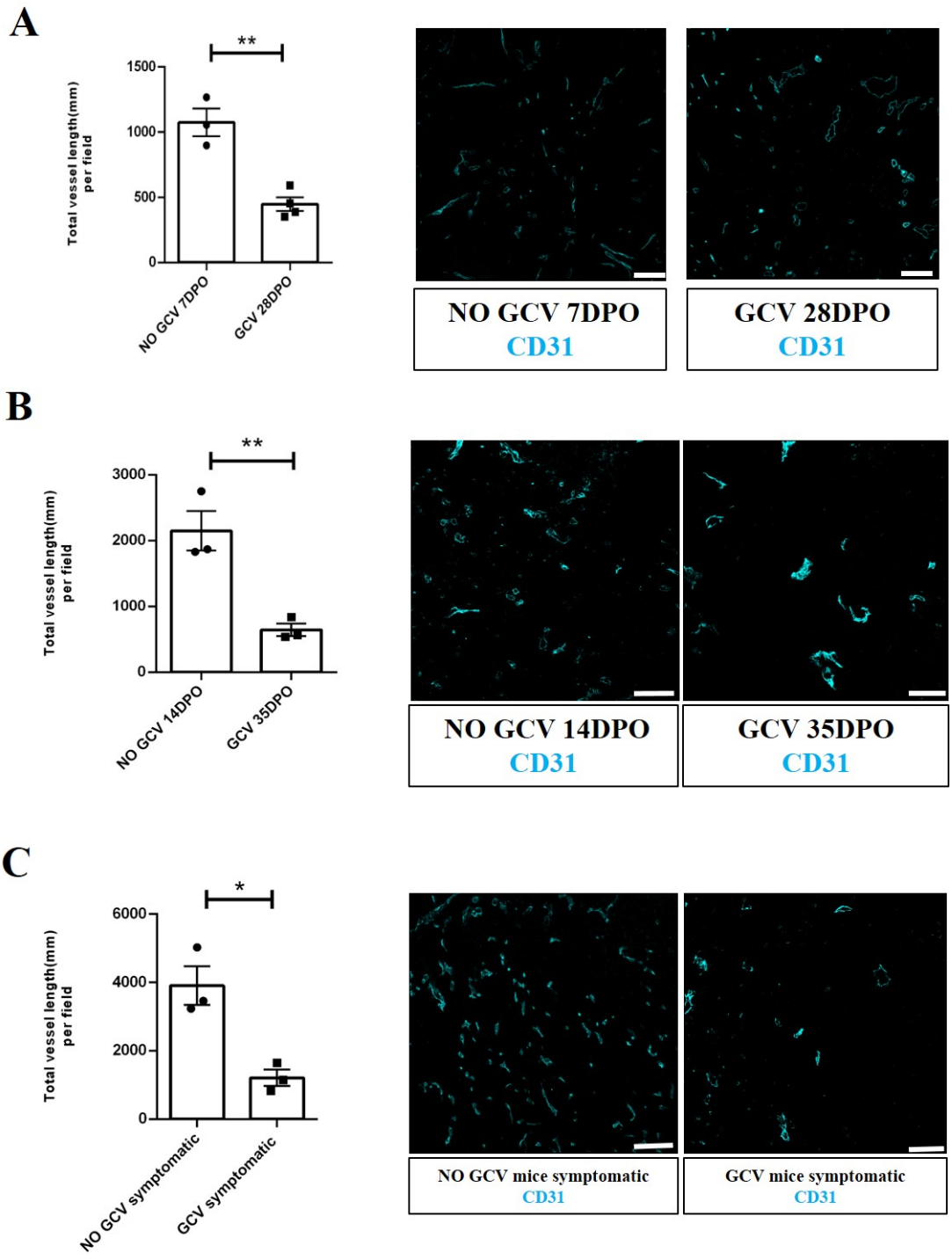

Figure 4.4.2 Recurrent GBM show decreased vascularization compared to primary GBM. (A) In the tumor growth early stage, total vessel length per area was quantified in the control (NO GCV 7DPO) and GCV-treated group (GCV 28DPO).

Representative images of immunostaining for CD31 showed fewer vessels in recurrent GBM than primary GBM. **(B)** In the tumor growth intermediate stage, the total vessel length per area in recurrent GBM (GCV 35DPO) was lower than in primary GBM (NO GCV 14DPO). Representative images of immunostaining for CD31 showed fewer vessels in recurrent GBM than primary GBM. **(C)** In the tumor growth late stage, the total vessel length per area in recurrent GBM (GCV symptomatic) was lower than in primary GBM (NO GCV symptomatic). Representative images of immunostaining for CD31 show fewer vessels in recurrent GBM than primary GBM. Statistical significance was calculated according to a Student's t-test, * $p < 0.05$, ** $p < 0.01$. Each dot represents one mouse. Values are reported as the mean ± SEM. The scale bars are 20 μm.

In summary, we established a new recurrent GBM mouse model, which recapitulated initial tumor growth, therapeutic reduction of tumor mass and subsequent tumor regrowth that is characterized for GBM recurrence. In our recurrent GBM model, it is more invasive and less angiogenic than primary GBM. Our GBM-relapse model could be used to explore the role of TAMEP during the GBM recurrence in the future research and might be used for research on the potential targets on recurrent GBM treatment.

5. Discussion

We discovered a novel cell population in the glioblastoma environment by using a lineage-tracing transgenic Nes-RFP mouse model. The traced RFP+ cells were initially divided into two subgroups (avascular RFP+ cells and vascular RFP+ cells) with respect to their localization in GBM. Purification of the traced avascular RFP+ cells and scRNAseq analysis of this population showed that they were a relatively homogenous cell population and their expression profile was different from other known cells of CNS. Bioinformatics analysis of scRNAseq data indicated their expression profile shared high similarity with microglia. FACS analysis showed the traced avascular RFP+ cells express myeloid cell marker CD11b in protein level. Their myeloid-like expression profile was confirmed by immunofluorescence, reporter mouse strain and FACS. SOX2, which is a crucial stem cell transcription factor and plays an important role in differentiation of neural stem/precursor cells[122], is expressed in the traced avascular RFP+ cell population but not in traced vascular RFP+ cells. After conditionally knocking out gene *Sox2* in traced avascular RFP+ cells, a much larger population of traced avascular RFP+ cells were reduced than only the population of initially characterized as SOX2-positive. Therefore, SOX2+ avascular RFP+ cells were the progenitor of traced avascular, myeloid-like cells and were necessary for maintaining the entire population of traced avascular cells [118]. In conclusion, these results revealed that the traced avascular RFP+ cells were a new and GBM-

parenchymal cell population (denominated as TAMEP).

However, the traced avascular RFP+ cells did not originate from established macrophages population including CNS-resident microglia and peripheral macrophages, which are both abundant in the glioblastoma microenvironment and share many markers[57, 65]. The Ionized calcium-binding adapter molecule 1 (Iba1) is an established marker of microglia/macrophages. However, Iba1 protein-expression was not detected in traced avascular RFP+ cells, distinguishing them from microglia and macrophages. Besides that, tumor-associated myeloid cells (assessed using the myeloid cell tracing model, *Cx3cr1*::creER2, R26-RFP) do not express Sox2 and consequently microglia/macrophages are not modulated by *Sox2*-knockout [118]. In contrast, TAMEP express SOX2 to a large extent and cell-type specific ablation of *Sox2* leads to TAMEP-depletion and strongly reduces GBM growth [118]. Altogether, this clearly supports our view that TAMEP did not derive from microglia. In addition, our experiment with bone-marrow chimera and lineage-reporting or lineage-tracing models clearly ruled out any contribution of the bone marrow monocyte-derived macrophages to the TAMEP cell-pool [118]. Suzuki et al. reported that Nestin is expressed in proliferative endothelial cells[130]. However, immunostaining for CD31 confirmed that traced avascular RFP+ cells were not endothelial cells. Furthermore, since we have determined that endothelial cells (assessed by *VE-cadherin*::creER2, R26-RFP) do not express SOX2 in GBM environment and conditional SOX2-loss in this model did not affect tumor expansion, they are unlikely to serve as a source for the traced avascular RFP+ cells in the Nes-RFP model.

Traced vascular RFP+ cells in the Nes-RFP model were identified as mature pericytes in glioblastoma because of their close association with endothelial cells and expression of PDGFRβ [131]. Pericytes play a vital role in glioblastoma growth and invasion by regulating the blood-brain barrier, promoting angiogenesis, and remodelling the extracellular matrix[132, 133]. Some studies have shown that pericytes have stemness potential and can differentiate into neural and myeloid lineages[134-136]. Using a pericyte lineage tracing model (*PDGFRβ*::creER2, R26-RFP), we showed that glioblastoma pericytes are negative for SOX2 and CD11b and are, therefore, not the source for the traced avascular RFP+ cells. Besides this, the result that conditional SOX2-loss in pericytes did not affect tumor size also confirmed pericytes are not the source of traced avascular RFP+ cells in Nes-RFP model. We also conducted intravital imaging of experimental GBM using two-photon microscopy to observe the movement of traced RFP+ cells [118]. We found that traced avascular and vascular RFP+ cells remained at their respective location throughout tumor growth. In particular, we observed no cell movement from vascular to avascular positions or from avascular to vascular positions. These results excluded that traced avascular RFP+ cells were pericyte progenitors or that TAMEP derived from pericytes which detached from vessels and differentiated into avascular RFP+ cells. We further found that the number of traced vascular RFP+ cells can constitute up to nearly 30% of all glioblastoma pericytes [118], suggesting that local progenitor cells can produce a large number of pericytes to support tumor growth. Although glioblastoma stem cells have been reported to differentiate into the majority of pericytes in the tumor tissue to assist tumor

growth and GSC self-renewal[90, 137], this is not an effect with any relevance for our study as our tracing model solely identified host-derived cell population. Additionally, some studies indicate that GSC-derived pericytes make only a tiny fraction of all intratumoral pericytes[42]. All in all, our experiments firmly indicated that TAMEP do not originate from microglia, endothelial cells, or pericytes.

In order to extend the detection of TAMEP to other mouse GBM models, human GBM or different tumor entities, we suggested that co-expression of SOX2 and PU.1 serves to identify TAMEP. We established that co-expression SOX2 and PU.1 in experimental brain tumors was restricted to TAMEP. Other research have previously shown that SOX2 and PU.1 would only co-expressed in some forms of leukemia, but not in physiology [129]. Both SOX2 and PU.1 are located in cell nucleus, so immunohistochemical detection of colocalization is a technically sound way for TAMEP identification. The existence of TAMEP in glioblastoma was not only detected in Nes-RFP mouse model, but independently confirmed in the *Sox2*::IRES-creER2, R26-RFP mouse model.

The quantity of TAMEP was abundant in early-stage tumor and decreased with tumor growth in our orthotopic GBM mouse model. How the number of TAMEP changes over time in different genetically engineered GBM mouse models still needs to be explored. We also observed that abundance of TAMEP is much higher in genetically engineered GBM model than in orthotopic GL261 tumor. One possible explanation is that tumorigenesis between genetically engineered GBM model and syngeneic GBM model is different. In our genetically engineered GBM model, specific genetic changes

including *Cdkn2a*-knockout and *PDGFB* upregulation lead to GBM formation. The number of TAMEP might be mainly modified by genes *Cdkn2a* and *PDGFB* or enriched in some GBM subgroups.

We also detected TAMEP in human glioblastoma tissue subject to a high level of inter- and intra-tumor heterogeneity of GBM. TAMEP could represent a potent regulator of tumor angiogenesis and glioblastoma expansion [118], making it a promising target for glioblastoma treatment. Thus, in the future, we will investigate how TAMEP regulate tumor angiogenesis in order to obtain new antiangiogenic target for glioblastoma treatment, especially in recurrent GBM. Because only a small portion of recurrent GBM patients could undergo re-operation and there is no standard and effective method for recurrent GBM treatment. Furthermore, detection of TAMEP in other brain tumors (medulloblastoma and metastatic brain tumors) extends the significance of our study to other brain tumors. Indeed, TAMEP are not detected in tumor-free brain or in models for stroke or neuro-inflammation, indicating that TAMEP might be specifically associated with different forms of brain tumors.

Recurrence in glioblastoma after treatment is almost unavoidable, which highly affect the patients' prognosis and survival[47]. However, there is no unified and highly effective method in recurrent glioblastoma treatment and lacking of recurrent GBM mouse model generating recurrent GBM of relevant anatomical location hinder the basic research for recurrent GBM. Therefore, establishing a recurrent GBM model for investigating the mechanisms underlying recurrence is of the utmost importance. Mitomu et al. reported a recurrent GBM mouse model[138] in which irradiating the

whole brain induced tumor regression[138]. However, this method is largely different from clinical recurrence after treatment. Usually, radiotherapy and chemotherapy are applied after maximal surgical dissection of GBM and irradiation is strictly directed toward identified tumor areas [139, 140]. Shinichi et al. also described patient-derived recurrent glioblastoma models[141] in which the cells injected into immune-deficient mice were derived from a relapsed glioblastoma after clinical treatment. However, this model does not recapitulate the initial tumor growth, therapeutic reduction of tumor mass and subsequent tumor regrowth that is characterized for GBM-relapse.

Since our study uses immunocompetent mice and shows well the process and characteristics of GBM recurrence, our model has clear advantages over the previously reported models. In our recurrent GBM models, both local and distant recurrence were observed, much like the clinical recurrence pattern[142]. However, the tumor size when mice were symptomatic in recurrent GBM mouse model was much smaller than tumor size in the primary GBM late stage. One possible explanation is that distant recurrence easily results in symptoms. For instance, the distant recurrence in the cerebellum will affect motor function [143]. Furthermore, recurrent GBM is less angiogenic and more invasive compared with primary GBM in our model. Because we detected TAMEP in recurrent GBM tissue, which implied TAMEP might play an important role in GBM recurrence and also promote angiogenesis during recurrence. Therefore, we aim to use this recurrent GBM model to investigate the role of TAMEP during GBM recurrence in the future. The reason why recurrent GBM became more invasive might be that some clones have acquired new pathological features, making tumor cells much more

invasive. Zagzag D et al. showed MHC class I and II genes were downregulated in invading GL261 tumor cells[144]. In our ongoing studies, we compare the gene profile between primary and recurrent GBM, also between GBM recurring locally or distant sites, which may help us understand the mechanism controlling invasiveness. All in all, our recurrent GBM mouse model could advance the understanding of recurrent glioblastoma heterogeneous features and mechanism, thus might providing novel directions for therapies of recurrent GBM.

6. Summary

Glioblastoma progression and recurrence are supported by cells in the tumor environment. The diversity of tumor-associated cells and the heterogeneity of glioblastoma all affect tumor therapy, prognosis, and support recurrence. In my MD Thesis, I investigated a novel cell population, termed TAMEP, and also established a new recurrent glioblastoma model. Because I detected TAMEP both in primary and recurrent human GBM tissue, this model also provides an opportunity to investigate the role of TAMEP in GBM relapse. Furthermore, the GBM-relapse model recapitulates important features of intratumoral heterogeneity, which can be exploited to develop important therapeutic concepts.

In the first part of my study, I traced two types of cells (vascular and avascular cell subpopulations) in glioblastoma using a transgenic lineage-tracing mouse model. Immunostaining for PDGFRβ (pericyte marker) and their close proximity to endothelial cells identified vascular RFP+ cells as mature pericytes. ScRNAseq analysis of traced avascular RFP+ cells in tumors suggested they are a relatively homogenous cell population without pericyte identity. Bioinformatics analysis indicated that the expression profile of traced avascular RFP+ cells is highly similar to microglia. FACS analysis and immunostaining results confirmed that traced avascular RFP+ cells express myeloid cell markers, such as CD11b and PU.1, but not Iba1. Sox2, as a crucial stem cell transcription factor, is expressed in part of the traced avascular RFP+ cells.

Conditional *Sox2*-loss in traced avascular RFP+ cells reduced a much larger population of traced avascular RFP+ cells than only the population initially characterized as SOX2-positive. Therefore, SOX2+ avascular RFP+ cells are the progenitor of traced avascular, myeloid-like cells and are necessary for maintaining the entire population of traced avascular cells. Using a series of cell lineage tracing models, I found that this traced cell population does not originate from microglia, endothelial cells, or pericytes. Thus, I described a new tumor-associated cell population with myeloid-like expression profile (termed as TAMEP).

TAMEP were detected in both human primary and recurrent glioblastoma, demonstrating the diversity of glioblastoma-associated cells. The finding that the number of TAMEP varies not only between different human GBM tissues but also between different areas in the same GBM-specimen indicates the loco-regional heterogeneity of TAMEP in GBM. TAMEP were also detected in human medulloblastoma and metastatic brain tumors, extending the significance of my study to other brain tumor types.

Recurrent glioblastomas often harbor different genetic mutations from the initial tumor. In order to investigate the heterogeneous features in recurrent glioblastoma, in the second part of my study, a new recurrent glioblastoma mouse model was established. Local and distant recurrence identified in this model showed a pattern similar to clinical observations. GBM can relapse at distant sites and this pathological feature was recapitulated by our GBM-relapse model. I also observed that these highly invasive recurrent GBM were less angiogenic than the primary tumors. This recurrent GBM

mouse model could advance the understanding of recurrent glioblastoma heterogeneous features. Furthermore, the GBM-relapse model can be used to explore the role of TAMEP during the GBM recurrence in future research, thus providing novel directions for therapies of recurrent GBM.

Zusammenfassung

Zellen des Tumorstromas unterstützen die Progression des Glioblastoms sowie dessen Wiederauftreten. Die verschiedenen tumorassoziierten Zellen und die Heterogenität der Tumorzellen beeinflussen Therapie, Prognose und unterstützen die Entstehung eines Tumorrezidivs. In meiner medizinischen Doktorarbeit habe ich eine neue Zellpopulation namens TAMEP untersucht und ein neues Mausmodell etabliert, um das Wiederauftreten von Glioblastomen zu untersuchen. Da ich TAMEP im primären als auch im rezidivierenden Glioblastom nachweisen konnte, schafft dieses Modell die Möglichkeit, die Rolle von TAMEP auch im rezidivierenden Glioblastom zu untersuchen. Weiterhin konnte ich zeigen, dass das Model wichtige Merkmale intratumoraler Heterogenität aufweist und so die Grundlage für wichtige therapeutische Ansätze schaffen kann.

Im ersten Teil meiner Studie detektierte ich mithilfe eines transgenen Mausmodels zwei verschiede Arten von Zellen in Glioblastomen: vaskuläre und avaskuläre Zell-Subpopulationen. Durch Immunfärbung von PDGFRβ (Perizytenmarker) und der unmittelbaren Nähe zu Endothelzellen konnten vaskuläre RFP+ Zellen als reife Perizyten identifiziert werden. In ScRNAseq Analysen zeigten sich die RFP+ Zellen als relativ homogene Zellpopulation ohne Perizytenidentität. Bioinformatische Analysen der Expressionsprofile wiesen darauf hin, dass avaskuläre RFP+ Zellen sehr ähnlich zu den Zellen der Mikroglia sind. In FACS-Analysen und Immunfärbungen konnte bestätigt werden, dass avaskuläre RFP+ Zellen myeloide Zellmarker, wie

CD11b und PU.1, nicht jedoch Iba1, exprimieren. Der bedeutende Transkriptionsfaktor Sox2 wird in einem Teil der avaskulären RFP+ Zellen exprimiert. Der bedingte Sox2-Verlust in den verfolgten avaskulären RFP + -Zellen reduzierte eine viel größere Population von avaskulärer RFP + -Zellen als nur die Anzahl von ursprünglich als SOX2-positiv charakterisierten Zellen. Die Sox2+ avaskulären RFP+ Zellen sind demnach Vorläuferzellen der detektierten myeloid-ähnlichen Zellen und daher notwendig, um die gesamte Population der avaskulären Zellen aufrecht zu halten. Unter Verwendung einer Reihe von Abstammungs-Modelle, konnte ich nachweisen, dass die detektierten Zellpopulationen weder von Perizyten noch von Zellen der Mikroglia oder des Endothels abstammen. Somit beschreiben ich hier eine neue tumorassoziierte myeloid-ähnlichen Zelltyp, genannt TAMEP.

TAMEP konnten sowohl in menschlichen primären als auch im rezidivierenden Glioblastom nachgewiesen werden, was die Zelldiversität des Glioblastoms sogar noch erweitert. Die Anzahl an TAMEP unterscheidet sich dabei nicht nur in unterschiedlichen Glioblastom-Patientenproben, sondern auch in verschiedenen Arealen in ein und demselben Tumor. Dies hebt die die lokoregionalee Heterogenität von TAMEP im Glioblastom hervor. TAMEP konnten auch im menschlichen Medulloblastom und in Hirnmetastasen verschiedenen Ursprungs nachgewiesen werden, was die Bedeutung von TAMEP auch für andere Tumore des Nervensystems verdeutlicht.

Oftmals unterscheidet sich das rezidivierende Glioblastom hinsichtlich seiner genetischen Mutationen vom ursprünglichen Tumor. Um die heterogenen Faktoren im

rezidiverenden Glioblastom zu untersuchuen, wurde im zweiten Teil meiner Dissertation ein neues Mausmodel etabliert. Glioblastomrezidive entstehen sowohl lokal als auch entfernt vom Ursprungsort im Gehirn. Dieses pathologische Merkmal wird in unserem Rezidivmodel wiedergespiegelt. Ich habe auch beobachtet, dass diese hochgradig invasiven rezidivierende GBM waren weniger angiogen als die Primärtumoren. Das Glioblastomrezidiv-Mausmodell könnte unser bisheriges Verständnis über das rezidivierende Glioblastom entscheidend verbessern. Weiterhin kann dieses Modell in zukünftigen Studien verwendet werden, um die Rolle von TAMEP während der Wiederkehr von Glioblastomen zu untersuchen. So könnten neue Therapieransätze für das rezidivierende Glioblastom entdeckt und untersucht werden.

7. Reference

1. Schwartzbaum, J.A., et al., *Epidemiology and molecular pathology of glioma.* Nature clinical practice. Neurology, 2006. **2**(9).
2. Ohgaki, H. and P. Kleihues, *Epidemiology and etiology of gliomas.* Acta neuropathologica, 2005. **109**(1).
3. Ostrom, Q.T., et al., *The epidemiology of glioma in adults: a "state of the science" review.* Neuro-oncology, 2014. **16**(7): p. 896-913.
4. Batash, R., et al., *Glioblastoma Multiforme, Diagnosis and Treatment; Recent Literature Review.* Current medicinal chemistry, 2017. **24**(27): p. 3002-3009.
5. Patel, A.P., et al., *Single-cell RNA-seq highlights intratumoral heterogeneity in primary glioblastoma.* Science (New York, N.Y.), 2014. **344**(6190): p. 1396-1401.
6. Parker, N.R., et al., *Intratumoral heterogeneity identified at the epigenetic, genetic and transcriptional level in glioblastoma.* Scientific reports, 2016. **6**: p. 22477.
7. Qazi, M.A., et al., *Intratumoral heterogeneity: pathways to treatment resistance and relapse in human glioblastoma.* Annals of oncology : official journal of the European Society for Medical Oncology, 2017. **28**(7): p. 1448-1456.
8. Walid, M.S., *Prognostic factors for long-term survival after glioblastoma.* The Permanente journal, 2008. **12**(4): p. 45-48.
9. Glas, M., et al., *Residual tumor cells are unique cellular targets in glioblastoma.* Annals of neurology, 2010. **68**(2): p. 264-269.
10. Louis, D.N., et al., *The 2016 World Health Organization Classification of Tumors of the Central Nervous System: a summary.* Acta neuropathologica, 2016. **131**(6): p. 803-820.
11. Ohgaki, H. and P. Kleihues, *The definition of primary and secondary glioblastoma.* Clinical cancer research : an official journal of the American Association for Cancer Research, 2013. **19**(4): p. 764-772.
12. Nobusawa, S., et al., *IDH1 mutations as molecular signature and predictive factor of secondary glioblastomas.* Clinical cancer research : an official journal of the American Association for Cancer Research, 2009. **15**(19): p. 6002-6007.
13. Balss, J., et al., *Analysis of the IDH1 codon 132 mutation in brain tumors.* Acta neuropathologica, 2008. **116**(6): p. 597-602.
14. Hartmann, C., et al., *Patients with IDH1 wild type anaplastic astrocytomas exhibit worse prognosis than IDH1-mutated glioblastomas, and IDH1 mutation status accounts for the unfavorable prognostic effect of higher age: implications for classification of gliomas.* Acta neuropathologica, 2010. **120**(6): p. 707-718.
15. Wen, W.X., A.J. Mead, and S. Thongjuea, *Technological advances and computational approaches for alternative splicing analysis in single cells.* Computational and structural biotechnology journal, 2020. **18**: p. 332-343.
16. *Comprehensive genomic characterization defines human glioblastoma genes and core pathways.* Nature, 2008. **455**(7216): p. 1061-1068.

17. Brennan, C.W., et al., *The somatic genomic landscape of glioblastoma.* Cell, 2013. **155**(2): p. 462-477.
18. Verhaak, R.G.W., et al., *Integrated genomic analysis identifies clinically relevant subtypes of glioblastoma characterized by abnormalities in PDGFRA, IDH1, EGFR, and NF1.* Cancer cell, 2010. **17**(1).
19. Van Meir, E.G., et al., *Exciting new advances in neuro-oncology: the avenue to a cure for malignant glioma.* CA: a cancer journal for clinicians, 2010. **60**(3): p. 166-193.
20. Hovinga, K.E., et al., *EGFR amplification and classical subtype are associated with a poor response to bevacizumab in recurrent glioblastoma.* Journal of neuro-oncology, 2019. **142**(2): p. 337-345.
21. Olar, A. and K.D. Aldape, *Using the molecular classification of glioblastoma to inform personalized treatment.* The Journal of pathology, 2014. **232**(2): p. 165-177.
22. Behnan, J., G. Finocchiaro, and G. Hanna, *The landscape of the mesenchymal signature in brain tumours.* Brain : a journal of neurology, 2019. **142**(4): p. 847-866.
23. Tran, A.N. and C. Horbinski, *Mesenchymal stemlike cells in glioblastoma.* Neuro-oncology, 2020. **22**(10): p. 1409-1410.
24. Alessandrini, F., et al., *Glioblastoma models driven by different mutations converge to the proneural subtype.* Cancer letters, 2020. **469**: p. 447-455.
25. Sidaway, P., *CNS cancer: Glioblastoma subtypes revisited.* Nature reviews. Clinical oncology, 2017. **14**(10): p. 587.
26. Brown, T.J., et al., *Association of the Extent of Resection With Survival in Glioblastoma: A Systematic Review and Meta-analysis.* JAMA oncology, 2016. **2**(11): p. 1460-1469.
27. Domino, J.S., et al., *Cytoreductive surgery in the management of newly diagnosed glioblastoma in adults: a systematic review and evidence-based clinical practice guideline update.* Journal of neuro-oncology, 2020. **150**(2): p. 121-142.
28. Quigley, M.R. and J.C. Maroon, *The relationship between survival and the extent of the resection in patients with supratentorial malignant gliomas.* Neurosurgery, 1991. **29**(3).
29. Lacroix, M., et al., *A multivariate analysis of 416 patients with glioblastoma multiforme: prognosis, extent of resection, and survival.* Journal of neurosurgery, 2001. **95**(2): p. 190-198.
30. Stupp, R., et al., *Radiotherapy plus concomitant and adjuvant temozolomide for glioblastoma.* The New England journal of medicine, 2005. **352**(10): p. 987-996.
31. Stupp, R., et al., *Effects of radiotherapy with concomitant and adjuvant temozolomide versus radiotherapy alone on survival in glioblastoma in a randomised phase III study: 5-year analysis of the EORTC-NCIC trial.* The Lancet. Oncology, 2009. **10**(5): p. 459-466.
32. Gilbert, M.R., et al., *Dose-dense temozolomide for newly diagnosed*

glioblastoma: a randomized phase III clinical trial. Journal of clinical oncology : official journal of the American Society of Clinical Oncology, 2013. **31**(32): p. 4085-4091.
33. Armstrong, T.S., et al., *Net clinical benefit analysis of radiation therapy oncology group 0525: a phase III trial comparing conventional adjuvant temozolomide with dose-intensive temozolomide in patients with newly diagnosed glioblastoma.* Journal of clinical oncology : official journal of the American Society of Clinical Oncology, 2013. **31**(32): p. 4076-4084.
34. Brada, M., et al., *Temozolomide versus procarbazine, lomustine, and vincristine in recurrent high-grade glioma.* Journal of clinical oncology : official journal of the American Society of Clinical Oncology, 2010. **28**(30): p. 4601-4608.
35. Young, J.S., et al., *Management of glioblastoma in elderly patients.* Journal of the neurological sciences, 2017. **380**: p. 250-255.
36. Friedman, H.S., et al., *Bevacizumab alone and in combination with irinotecan in recurrent glioblastoma.* Journal of clinical oncology : official journal of the American Society of Clinical Oncology, 2009. **27**(28): p. 4733-4740.
37. Rominiyi, O., et al., *Tumour treating fields therapy for glioblastoma: current advances and future directions.* British journal of cancer, 2020.
38. Khasraw, M., et al., *Antiangiogenic therapy for high-grade glioma.* The Cochrane database of systematic reviews, 2014(9): p. CD008218.
39. Carrieri, F.A., et al., *Tumor Treating Fields: At the Crossroads Between Physics and Biology for Cancer Treatment.* Frontiers in oncology, 2020. **10**: p. 575992.
40. Stupp, R., et al., *Maintenance Therapy With Tumor-Treating Fields Plus Temozolomide vs Temozolomide Alone for Glioblastoma: A Randomized Clinical Trial.* JAMA, 2015. **314**(23): p. 2535-2543.
41. Stupp, R., et al., *Effect of Tumor-Treating Fields Plus Maintenance Temozolomide vs Maintenance Temozolomide Alone on Survival in Patients With Glioblastoma: A Randomized Clinical Trial.* JAMA, 2017. **318**(23): p. 2306-2316.
42. Svensson, A., et al., *Endogenous brain pericytes are widely activated and contribute to mouse glioma microvasculature.* PloS one, 2015. **10**(4): p. e0123553.
43. Burger, P.C., et al., *Computerized tomographic and pathologic studies of the untreated, quiescent, and recurrent glioblastoma multiforme.* Journal of neurosurgery, 1983. **58**(2): p. 159-169.
44. De Bonis, P., et al., *The influence of surgery on recurrence pattern of glioblastoma.* Clinical neurology and neurosurgery, 2013. **115**(1): p. 37-43.
45. van Nifterik, K.A., et al., *Genetic profiling of a distant second glioblastoma multiforme after radiotherapy: Recurrence or second primary tumor?* Journal of neurosurgery, 2006. **105**(5): p. 739-744.
46. Birzu, C., et al., *Recurrent Glioblastoma: From Molecular Landscape to New Treatment Perspectives.* Cancers, 2020. **13**(1).
47. Campos, B., et al., *A comprehensive profile of recurrent glioblastoma.* Oncogene, 2016. **35**(45): p. 5819-5825.

48. Woodroffe, R.W., et al., *Survival after reoperation for recurrent glioblastoma.* Journal of clinical neuroscience : official journal of the Neurosurgical Society of Australasia, 2020. **73**: p. 118-124.
49. Di Nunno, V., et al., *Treatment of recurrent glioblastoma: state-of-the-art and future perspectives.* Expert review of anticancer therapy, 2020. **20**(9): p. 785-795.
50. Wang, J., et al., *Clonal evolution of glioblastoma under therapy.* Nature genetics, 2016. **48**(7): p. 768-776.
51. Kim, J., et al., *Spatiotemporal Evolution of the Primary Glioblastoma Genome.* Cancer cell, 2015. **28**(3): p. 318-328.
52. Kim, H., et al., *Whole-genome and multisector exome sequencing of primary and post-treatment glioblastoma reveals patterns of tumor evolution.* Genome research, 2015. **25**(3): p. 316-327.
53. Tully, P.A., et al., *Reoperation for Recurrent Glioblastoma and Its Association With Survival Benefit.* Neurosurgery, 2016. **79**(5): p. 678-689.
54. Broekman, M.L., et al., *Multidimensional communication in the microenvirons of glioblastoma.* Nature reviews. Neurology, 2018. **14**(8): p. 482-495.
55. Touat, M., et al., *Glioblastoma targeted therapy: updated approaches from recent biological insights.* Annals of oncology : official journal of the European Society for Medical Oncology, 2017. **28**(7): p. 1457-1472.
56. Takano, T., et al., *Glutamate release promotes growth of malignant gliomas.* Nature medicine, 2001. **7**(9): p. 1010-1015.
57. Poon, C.C., et al., *Glioblastoma-associated microglia and macrophages: targets for therapies to improve prognosis.* Brain : a journal of neurology, 2017. **140**(6): p. 1548-1560.
58. Mega, A., et al., *Astrocytes enhance glioblastoma growth.* Glia, 2020. **68**(2): p. 316-327.
59. Mathivet, T., et al., *Dynamic stroma reorganization drives blood vessel dysmorphia during glioma growth.* EMBO molecular medicine, 2017. **9**(12): p. 1629-1645.
60. Müller, A., et al., *Resident microglia, and not peripheral macrophages, are the main source of brain tumor mononuclear cells.* International journal of cancer, 2015. **137**(2): p. 278-288.
61. Butovsky, O. and H.L. Weiner, *Microglial signatures and their role in health and disease.* Nature reviews. Neuroscience, 2018. **19**(10): p. 622-635.
62. Ginhoux, F., et al., *Fate mapping analysis reveals that adult microglia derive from primitive macrophages.* Science (New York, N.Y.), 2010. **330**(6005): p. 841-845.
63. Biber, K., et al., *Central nervous system myeloid cells as drug targets: current status and translational challenges.* Nature reviews. Drug discovery, 2016. **15**(2): p. 110-124.
64. Glass, R. and M. Synowitz, *CNS macrophages and peripheral myeloid cells in brain tumours.* Acta neuropathologica, 2014. **128**(3): p. 347-362.
65. Hambardzumyan, D., D.H. Gutmann, and H. Kettenmann, *The role of microglia*

and macrophages in glioma maintenance and progression. Nature neuroscience, 2016. **19**(1): p. 20-27.
66. Hickman, S.E., et al., *The microglial sensome revealed by direct RNA sequencing.* Nature neuroscience, 2013. **16**(12): p. 1896-1905.
67. Ford, A.L., et al., *Microglia induce CD4 T lymphocyte final effector function and death.* The Journal of experimental medicine, 1996. **184**(5): p. 1737-1745.
68. Badie, B. and J.M. Schartner, *Flow cytometric characterization of tumor-associated macrophages in experimental gliomas.* Neurosurgery, 2000. **46**(4).
69. Zrzavy, T., et al., *Pro-inflammatory activation of microglia in the brain of patients with sepsis.* Neuropathology and applied neurobiology, 2019. **45**(3): p. 278-290.
70. Pluvinage, J.V., et al., *CD22 blockade restores homeostatic microglial phagocytosis in ageing brains.* Nature, 2019. **568**(7751): p. 187-192.
71. Masuda, T., et al., *Novel Hexb-based tools for studying microglia in the CNS.* Nature immunology, 2020. **21**(7): p. 802-815.
72. Goldmann, T., et al., *A new type of microglia gene targeting shows TAK1 to be pivotal in CNS autoimmune inflammation.* Nature neuroscience, 2013. **16**(11): p. 1618-1626.
73. Schulz, C., et al., *A lineage of myeloid cells independent of Myb and hematopoietic stem cells.* Science (New York, N.Y.), 2012. **336**(6077): p. 86-90.
74. Li, W. and M.B. Graeber, *The molecular profile of microglia under the influence of glioma.* Neuro-oncology, 2012. **14**(8): p. 958-978.
75. Zhou, W., et al., *Periostin secreted by glioblastoma stem cells recruits M2 tumour-associated macrophages and promotes malignant growth.* Nature cell biology, 2015. **17**(2): p. 170-182.
76. Ye, X.-z., et al., *Tumor-associated microglia/macrophages enhance the invasion of glioma stem-like cells via TGF-β1 signaling pathway.* Journal of immunology (Baltimore, Md. : 1950), 2012. **189**(1): p. 444-453.
77. Singh, S.K., et al., *Identification of human brain tumour initiating cells.* Nature, 2004. **432**(7015): p. 396-401.
78. Lathia, J.D., et al., *Cancer stem cells in glioblastoma.* Genes & development, 2015. **29**(12): p. 1203-1217.
79. van Hinsbergh, V.W.M. and P. Koolwijk, *Endothelial sprouting and angiogenesis: matrix metalloproteinases in the lead.* Cardiovascular research, 2008. **78**(2): p. 203-212.
80. Tabatabai, G., et al., *Lessons from the bone marrow: how malignant glioma cells attract adult haematopoietic progenitor cells.* Brain : a journal of neurology, 2005. **128**(Pt 9): p. 2200-2211.
81. Chen, X., et al., *RAGE expression in tumor-associated macrophages promotes angiogenesis in glioma.* Cancer research, 2014. **74**(24): p. 7285-7297.
82. Ahir, B.K., H.H. Engelhard, and S.S. Lakka, *Tumor Development and Angiogenesis in Adult Brain Tumor: Glioblastoma.* Molecular neurobiology, 2020. **57**(5): p. 2461-2478.
83. Wesseling, P., D.J. Ruiter, and P.C. Burger, *Angiogenesis in brain tumors;*

pathobiological and clinical aspects. Journal of neuro-oncology, 1997. **32**(3): p. 253-265.
84. Sharma, A. and A. Shiras, *Cancer stem cell-vascular endothelial cell interactions in glioblastoma.* Biochemical and biophysical research communications, 2016. **473**(3): p. 688-692.
85. Treps, L., et al., *Glioblastoma stem-like cells secrete the pro-angiogenic VEGF-A factor in extracellular vesicles.* Journal of extracellular vesicles, 2017. **6**(1): p. 1359479.
86. Bao, S., et al., *Stem cell-like glioma cells promote tumor angiogenesis through vascular endothelial growth factor.* Cancer research, 2006. **66**(16): p. 7843-7848.
87. Lang, H.L., et al., *Glioma cells promote angiogenesis through the release of exosomes containing long non-coding RNA POU3F3.* European review for medical and pharmacological sciences, 2017. **21**(5): p. 959-972.
88. Baisiwala, S., et al., *Chemotherapeutic Stress Induces Transdifferentiation of Glioblastoma Cells to Endothelial Cells and Promotes Vascular Mimicry.* Stem cells international, 2019. **2019**: p. 6107456.
89. Soda, Y., et al., *Transdifferentiation of glioblastoma cells into vascular endothelial cells.* Proceedings of the National Academy of Sciences of the United States of America, 2011. **108**(11): p. 4274-4280.
90. Cheng, L., et al., *Glioblastoma stem cells generate vascular pericytes to support vessel function and tumor growth.* Cell, 2013. **153**(1): p. 139-152.
91. Schmidt, N.O., et al., *Levels of vascular endothelial growth factor, hepatocyte growth factor/scatter factor and basic fibroblast growth factor in human gliomas and their relation to angiogenesis.* International journal of cancer, 1999. **84**(1): p. 10-18.
92. Weathers, S.-P. and J. de Groot, *VEGF Manipulation in Glioblastoma.* Oncology (Williston Park, N.Y.), 2015. **29**(10): p. 720-727.
93. Jain, R.K., *Molecular regulation of vessel maturation.* Nature medicine, 2003. **9**(6): p. 685-693.
94. Arvanitis, C.D., G.B. Ferraro, and R.K. Jain, *The blood-brain barrier and blood-tumour barrier in brain tumours and metastases.* Nature reviews. Cancer, 2020. **20**(1): p. 26-41.
95. Peterson, T.E., et al., *Dual inhibition of Ang-2 and VEGF receptors normalizes tumor vasculature and prolongs survival in glioblastoma by altering macrophages.* Proceedings of the National Academy of Sciences of the United States of America, 2016. **113**(16): p. 4470-4475.
96. Dubois, L.G., et al., *Gliomas and the vascular fragility of the blood brain barrier.* Frontiers in cellular neuroscience, 2014. **8**: p. 418.
97. van Tellingen, O., et al., *Overcoming the blood-brain tumor barrier for effective glioblastoma treatment.* Drug resistance updates : reviews and commentaries in antimicrobial and anticancer chemotherapy, 2015. **19**.
98. Calzascia, T., et al., *Homing phenotypes of tumor-specific CD8 T cells are predetermined at the tumor site by crosspresenting APCs.* Immunity, 2005.

22(2): p. 175-184.
99. Iwadate, Y., et al., *Intrinsic protective mechanisms of the neuron-glia network against glioma invasion.* Journal of clinical neuroscience : official journal of the Neurosurgical Society of Australasia, 2016. **26**: p. 19-25.
100. Venkatesh, H.S., et al., *Targeting neuronal activity-regulated neuroligin-3 dependency in high-grade glioma.* Nature, 2017. **549**(7673): p. 533-537.
101. Sottoriva, A., et al., *Intratumor heterogeneity in human glioblastoma reflects cancer evolutionary dynamics.* Proceedings of the National Academy of Sciences of the United States of America, 2013. **110**(10): p. 4009-4014.
102. Gerlinger, M., et al., *Intratumor heterogeneity and branched evolution revealed by multiregion sequencing.* The New England journal of medicine, 2012. **366**(10): p. 883-892.
103. Inda, M.-D.-M., R. Bonavia, and J. Seoane, *Glioblastoma multiforme: a look inside its heterogeneous nature.* Cancers, 2014. **6**(1): p. 226-239.
104. Bonavia, R., et al., *Heterogeneity maintenance in glioblastoma: a social network.* Cancer research, 2011. **71**(12): p. 4055-4060.
105. Pires-Afonso, Y., S.P. Niclou, and A. Michelucci, *Revealing and Harnessing Tumour-Associated Microglia/Macrophage Heterogeneity in Glioblastoma.* International journal of molecular sciences, 2020. **21**(3).
106. Müller, S., et al., *Single-cell profiling of human gliomas reveals macrophage ontogeny as a basis for regional differences in macrophage activation in the tumor microenvironment.* Genome biology, 2017. **18**(1): p. 234.
107. Darmanis, S., et al., *Single-Cell RNA-Seq Analysis of Infiltrating Neoplastic Cells at the Migrating Front of Human Glioblastoma.* Cell reports, 2017. **21**(5): p. 1399-1410.
108. Nickel, G.C., et al., *Characterizing mutational heterogeneity in a glioblastoma patient with double recurrence.* PloS one, 2012. **7**(4): p. e35262.
109. Magee, J.A., E. Piskounova, and S.J. Morrison, *Cancer stem cells: impact, heterogeneity, and uncertainty.* Cancer cell, 2012. **21**(3): p. 283-296.
110. Eskilsson, E., et al., *EGFRvIII mutations can emerge as late and heterogenous events in glioblastoma development and promote angiogenesis through Src activation.* Neuro-oncology, 2016. **18**(12): p. 1644-1655.
111. Osuka, S. and E.G. Van Meir, *Overcoming therapeutic resistance in glioblastoma: the way forward.* The Journal of clinical investigation, 2017. **127**(2): p. 415-426.
112. Wei, W., et al., *Single-Cell Phosphoproteomics Resolves Adaptive Signaling Dynamics and Informs Targeted Combination Therapy in Glioblastoma.* Cancer cell, 2016. **29**(4): p. 563-573.
113. Valny, M., et al., *Tamoxifen in the Mouse Brain: Implications for Fate-Mapping Studies Using the Tamoxifen-Inducible Cre-loxP System.* Frontiers in cellular neuroscience, 2016. **10**: p. 243.
114. Hayashi, S. and A.P. McMahon, *Efficient recombination in diverse tissues by a tamoxifen-inducible form of Cre: a tool for temporally regulated gene activation/inactivation in the mouse.* Developmental biology, 2002. **244**(2): p.

305-318.
115. Feil, R., et al., *Regulation of Cre recombinase activity by mutated estrogen receptor ligand-binding domains.* Biochemical and biophysical research communications, 1997. **237**(3): p. 752-757.
116. Mattioni, T., J.F. Louvion, and D. Picard, *Regulation of protein activities by fusion to steroid binding domains.* Methods in cell biology, 1994. **43 Pt A**: p. 335-352.
117. Frisch, A., et al., *Apelin Controls Angiogenesis-Dependent Glioblastoma Growth.* International journal of molecular sciences, 2020. **21**(11).
118. Kälin, R.E., et al., *TAMEP are brain tumor parenchymal cells controlling neoplastic angiogenesis and progression.* Cell systems, 2021.
119. Bondjers, C., et al., *Microarray analysis of blood microvessels from PDGF-B and PDGF-Rbeta mutant mice identifies novel markers for brain pericytes.* FASEB journal : official publication of the Federation of American Societies for Experimental Biology, 2006. **20**(10): p. 1703-1705.
120. Zeisel, A., et al., *Brain structure. Cell types in the mouse cortex and hippocampus revealed by single-cell RNA-seq.* Science (New York, N.Y.), 2015. **347**(6226): p. 1138-1142.
121. Back, J., et al., *Visualizing PU.1 activity during hematopoiesis.* Experimental hematology, 2005. **33**(4): p. 395-402.
122. Garros-Regulez, L., et al., *Targeting SOX2 as a Therapeutic Strategy in Glioblastoma.* Front Oncol, 2016.
123. Wieghofer, P., K.-P. Knobeloch, and M. Prinz, *Genetic targeting of microglia.* Glia, 2015. **63**(1).
124. Parkhurst, C.N., et al., *Microglia promote learning-dependent synapse formation through brain-derived neurotrophic factor.* Cell, 2013. **155**(7): p. 1596-1609.
125. Monvoisin, A., et al., *VE-cadherin-CreERT2 transgenic mouse: a model for inducible recombination in the endothelium.* Developmental dynamics : an official publication of the American Association of Anatomists, 2006. **235**(12): p. 3413-3422.
126. Cuervo, H., et al., *PDGFRβ-P2A-CreER mice: a genetic tool to target pericytes in angiogenesis.* Angiogenesis, 2017. **20**(4): p. 655-662.
127. Riccardi, S., et al., *MiR-210 promotes sensory hair cell formation in the organ of corti.* BMC genomics, 2016. **17**: p. 309.
128. Jung, S., et al., *Analysis of fractalkine receptor CX(3)CR1 function by targeted deletion and green fluorescent protein reporter gene insertion.* Molecular and cellular biology, 2000. **20**(11): p. 4106-4114.
129. Tosic, N., et al., *Prognostic significance of SOX2, SOX3, SOX11, SOX14 and SOX18 gene expression in adult de novo acute myeloid leukemia.* Leukemia research, 2018. **67**: p. 32-38.
130. Suzuki, S., et al., *The neural stem/progenitor cell marker nestin is expressed in proliferative endothelial cells, but not in mature vasculature.* The journal of histochemistry and cytochemistry : official journal of the Histochemistry

Society, 2010. **58**(8): p. 721-730.
131. Winkler, E.A., R.D. Bell, and B.V. Zlokovic, *Pericyte-specific expression of PDGF beta receptor in mouse models with normal and deficient PDGF beta receptor signaling.* Molecular neurodegeneration, 2010. **5**: p. 32.
132. Jackson, S., et al., *Blood-brain barrier pericyte importance in malignant gliomas: what we can learn from stroke and Alzheimer's disease.* Neuro-oncology, 2017. **19**(9): p. 1173-1182.
133. Sweeney, M.D., S. Ayyadurai, and B.V. Zlokovic, *Pericytes of the neurovascular unit: key functions and signaling pathways.* Nature neuroscience, 2016. **19**(6): p. 771-783.
134. Armulik, A., G. Genové, and C. Betsholtz, *Pericytes: developmental, physiological, and pathological perspectives, problems, and promises.* Developmental cell, 2011. **21**(2): p. 193-215.
135. Birbrair, A., et al., *How Plastic Are Pericytes?* Stem cells and development, 2017. **26**(14): p. 1013-1019.
136. Birbrair, A., et al., *Pericytes at the intersection between tissue regeneration and pathology.* Clinical science (London, England : 1979), 2015. **128**(2): p. 81-93.
137. Caspani, E.M., et al., *Glioblastoma: a pathogenic crosstalk between tumor cells and pericytes.* PloS one, 2014. **9**(7): p. e101402.
138. Kioi, M., et al., *Inhibition of vasculogenesis, but not angiogenesis, prevents the recurrence of glioblastoma after irradiation in mice.* The Journal of clinical investigation, 2010. **120**(3): p. 694-705.
139. Aizer, A.A., et al., *Underutilization of radiation therapy in patients with glioblastoma: predictive factors and outcomes.* Cancer, 2014. **120**(2): p. 238-243.
140. Sulman, E.P., et al., *Radiation Therapy for Glioblastoma: American Society of Clinical Oncology Clinical Practice Guideline Endorsement of the American Society for Radiation Oncology Guideline.* Journal of clinical oncology : official journal of the American Society of Clinical Oncology, 2017. **35**(3): p. 361-369.
141. Esaki, S., et al., *Blockade of transforming growth factor-β signaling enhances oncolytic herpes simplex virus efficacy in patient-derived recurrent glioblastoma models.* International journal of cancer, 2017. **141**(11): p. 2348-2358.
142. Jungk, C., et al., *Location-Dependent Patient Outcome and Recurrence Patterns in IDH1-Wildtype Glioblastoma.* Cancers, 2019. **11**(1).
143. Pfiffner, T.J., R. Jani, and L. Mechtler, *Neuro-oncological disorders of the cerebellum.* Neurologic clinics, 2014. **32**(4): p. 913-941.
144. Zagzag, D., et al., *Downregulation of major histocompatibility complex antigens in invading glioma cells: stealth invasion of the brain.* Laboratory investigation; a journal of technical methods and pathology, 2005. **85**(3): p. 328-341.

8. Acknowledgement

My first and sincere appreciation goes to Prof. Dr. Rainer Glass, my supervisor for his continuous support, extraordinary help and constructive advice in all stages of my doctoral studies. Thanks for supporting my every research project, for always encourage me to have a try. Especially thanks for funding me in the last year of my study. Without his help and support, I could not have done it. As excellent scientists, his profound knowledge, serious attitude and rigorous thinking really impressed me. I benefited a lot from him and these will be also very helpful for my future work.

I am also very grateful for the help and support from my co-supervisor Dr. Roland Kaelin. Thanks for his suggestions and comments every time after each experiment and always answering my questions patiently. I am particularly grateful to Ms. Stefanie Lange for her technical support during my research and also her assistance for my life in Munich. Moreover, great thanks to other members of neurosurgical research group: Mr. Min Li, Mr. Huabin Zhang, Ms. Jiying Cheng, Mr. Linzhi Cai, Mr. Enio Barci, Dr. Sabrina V Kirchleitner, Ms. Lena Schumacher, Ms. Lisa Niederauer, Mr. Robin Wechter, Mr. Sven Richter and Mr. Fabian Binter, for spending nice time together with me during my study time.

I also want to express my gratitude to Dr. Steffen Dietzel and Dr. Andreas Thomas, for their technical support on confocal microscope. Many thanks to our collaborators, Prof. Wolfgang Enard, Dr. Ines Hellmann and Mr. Philipp Janseen for their help and allowing me to use the bioinformatical figures in my thesis.

I also want to thank all my friends in Munich. We spent lots of happy time together.

Furthermore, I am very grateful the help and support from my master supervisor Prof. Bao Yinghui. Also, I gratefully thank the help from Prof. Zhang Xiaohua, Prof. Wang Yong and Dr. Gao Weizhen. Thanks to China Scholarship Council for providing me financial support.

Last but not the least, I would like to express my gratitude for their endless love and continued support. Especially my wife Ms. Yu Bingwen, she came to Germany to accompany me through these unforgettable days and made me believe life is beautiful. Thanks to my father, my mother and my sister. You always encourage me to support my dream during the past years. Your love and support meaned the world to me!